

## Article

# Application of Novel Concrete-Filled Built-Up K-Joints with Different Brace Sections in a Double-Deck Truss Bridge with a Symmetric Deck System with Dense Crossbeams

Mampiandra N. H. Zafimandimby, Yongjian Liu \*, Lei Jiang \* and Xindong Zhao

School of Highway, Chang'an University, Xi'an 710064, China; 2018021901@chd.edu.cn (M.N.H.Z.); zhaoxindong@chd.edu.cn (X.Z.)

\* Correspondence: liuyongjian@chd.edu.cn (Y.L.); jiangleichd@chd.edu.cn (L.J.)

**Abstract:** To facilitate the first application of the novel concrete-filled built-up K-joints with different brace sections in truss bridges, the present paper aims to determine their practicability through a comparison with integral joints. First, a structural analysis was carried out using the MIDAS CIVIL software to evaluate the loading applied to the structure. Additionally, boundary condition analysis was carried out. After that, the symmetric multi-planar joints were developed, using Abaqus 6.14 for the strength verification and the failure mode identification. These were followed by the multi-planar joints estimate cost. The results indicated that for positive bending, the novel joint deformed by 2.01 mm, compared to 4.83 mm for the integral joint in the serviceability limit state. These deformations were equal to 5.58 mm and 7.68 mm, respectively, in the negative bending. Verification under the ultimate limit state indicated a deformation of 10.43 mm for the novel joint type and 16.59 mm for the integral joint in the positive bending, whereas deformations of 15.89 mm and 16.82 mm were indicated in the negative bending. Moreover, a failure mode analysis showed a buckling of the arc yielding for the novel joint type and a buckling of the gusset plate for the integral joint. Finally, the results showed that the novel type of joint was more expensive by about CNY 111,286.06.



**Citation:** Zafimandimby, M.N.H.; Liu, Y.; Jiang, L.; Zhao, X. Application of Novel Concrete-Filled Built-Up K-Joints with Different Brace Sections in a Double-Deck Truss Bridge with a Symmetric Deck System with Dense Crossbeams. *Symmetry* **2023**, *15*, 1876. <https://doi.org/10.3390/sym15101876>

Academic Editor: Igor V. Andrianov

Received: 2 August 2023

Revised: 16 September 2023

Accepted: 22 September 2023

Published: 6 October 2023



**Copyright:** © 2023 by the authors. Licensee MDPI, Basel, Switzerland. This article is an open access article distributed under the terms and conditions of the Creative Commons Attribution (CC BY) license (<https://creativecommons.org/licenses/by/4.0/>).

**Keywords:** novel joint type; integral joint; symmetric dense crossbeams; multi-planar strength; strength comparison; estimate cost

## 1. Introduction

Truss structures are commonly used in beam bridges, suspension bridges, cable-stayed bridges, and arch bridges. A concrete-filled steel tube (CFST) is a type of strengthening that improves the overall truss resistance, including the initial stiffness [1], ultimate strength [2,3], and joint fatigue performance. Due to these benefits, the number of CFST bridges in China has grown over the last twenty years [4]. Since joints are the weakest part of truss structures, several codes, such as CIDECT [5] and Eurocodes [6], deal with hollow-section joints [7–12]. Moreover, several studies have address strengthening in order to retrofit hollow-section joints. One of the most relevant is carried out by Mampiandra N.H. Zafimandimby et al. [2] for classification and comparison.

Novel concrete-filled built-up K-joints with different brace sections represent a new type of joint designed to be the compression brace member in a rectangular hollow section with a brace-to-chord-width ratio  $\beta < 0.8$ . The tension brace is an open section that is directly welded to the chord member (Figure 1). This geometry raises the possibility of a negative gap in the structure, which increases its strength. More precisely, an analysis carried out by Mampiandra et al. [13] indicated that this novel joint type is stronger than a rectangular hollow-section (RHS) joint by 3% to 6% in terms of its initial stiffness and by around 10% in terms of its ultimate strength. Therefore, the novel joint was recommended

for use in truss bridges, especially of the Warren type because of its adequacy in the geometry [13].

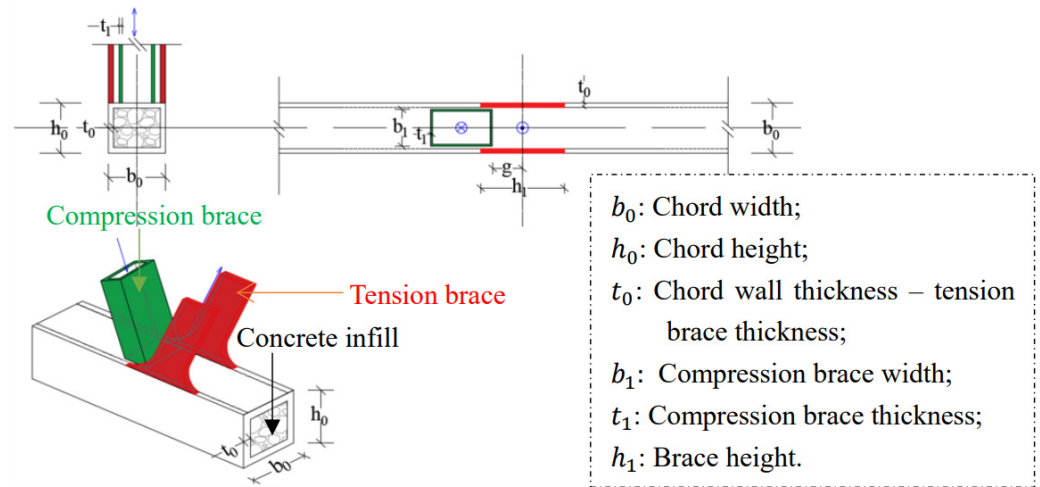


Figure 1. Novel concrete-filled built-up section with different brace sections [13].

In the cross-section, the trusses in bridges are connected through the crossbeams, which are generally positioned in the middle of the joints. In addition, the truss is retrofitted using a longitudinal crossbeam to carry the applied load so as to avoid bending, or even failure of the transversal type. This system has been proven to be satisfactory for the trusses of beam bridges [14,15], arch bridges [16,17], suspension bridges [18,19], and cable-stayed bridges [20,21]. A new deck system design is used in the Xi'an Weihe bridge that consists of several crossbeams, including in the joints and in the intermediates (Figure 2). In addition to that, no longitudinal crossbeam is applied. The main advantage of this design is that loading is directly transferred to the truss chord members, which are the strongest components in the truss structure. However, the presence of intermediate crossbeams creates another type of loading, which is mainly divided as the in-plane bending and the out-of-plane bending.

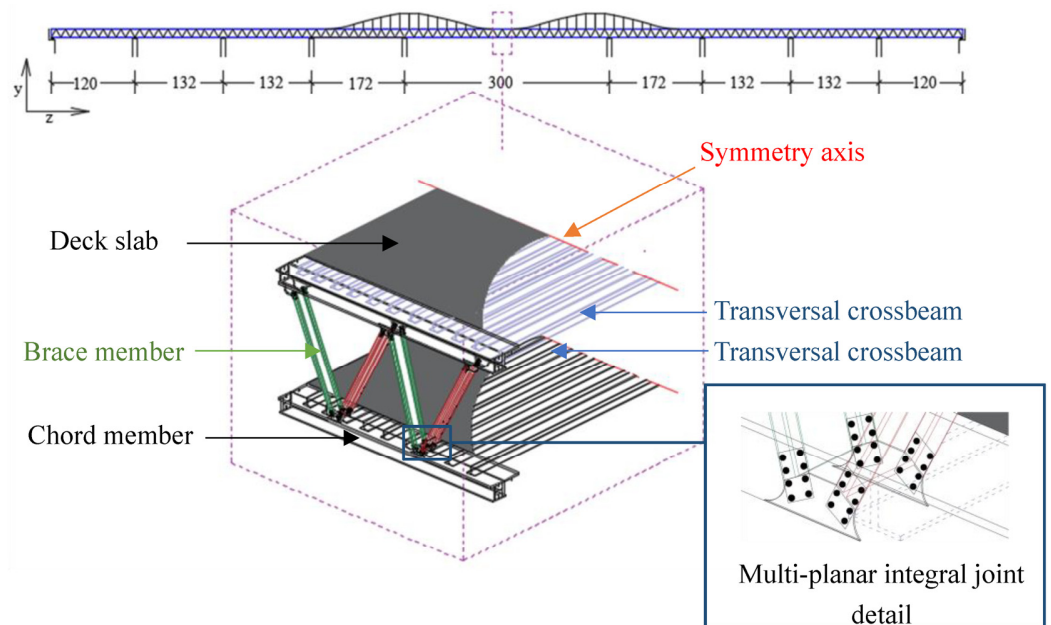


Figure 2. Multi-planar concept of the Xi'an Weihe bridge.

To date, the analysis of the novel joint type has focused solely on single joints [13], and no study has been carried out concerning the multi-planar dense-crossbeam deck system. Therefore, the present paper aims to apply the concrete-filled built-up-section K-joints with different brace sections to the Xi'an Weihe bridge, with its symmetric dense-crossbeam system, to check its strength and perform a failure mode analysis. Moreover, an estimate cost of the multi-planar joints in positive bending and negative bending is a target. The first section describes the Xi'an Weihe bridge and the novel concrete-filled built-up K-joints with different brace sections. Then, the second section offers a structural analysis of the bridge and conducts strength checking. The third section offers an analysis of the multi-planar dense-crossbeam failure mode for its ultimate capacity. The final section is related to the estimated cost analysis of the novel joint and the integral joint under positive and the negative bending.

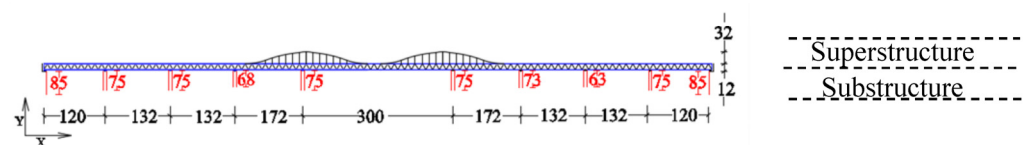
## 2. Overview of the Xi'an Weihe Bridge and Its Joints

### 2.1. Introduction to the Xi'an Weihe Bridge

Historically, double-deck truss bridges have been developed and used in China since 1937 for vehicle roads and railway lines. Several bridges have been built in this style, for example, the Qiantang River Bridge in 1937, the Wuhan double-deck bridge in 1957, the Dongjiang Bridge in 2009, the Dashengguan Yangtze River Bridge in 2011, and the Jinan Yellow River double-deck bridge in 2020. At present, Xi'an is undergoing another construction project: a double-deck truss bridge for subway line 10 across the Weihe river with a total length of 1412 m, composed of nine spans: 120 m + 2 × 132 m + 172 m + 300 m + 172 m + 2 × 132 m + 120 m (Figure 3). Transversally, the height of the truss structure is 12 m and the width of the cross-section is 39.8 m, composed of 4.65 m sidewalks on both sides and two vehicle lanes of 8.5 m, combined with railway lanes of 13.5 m in the lower deck and six vehicle lanes in the upper deck. The bridge project was designed according to the Chinese standard for both subways and highways, including the code for the design of metros (GB 50157-2013) [22], the code for design of railway lines (GB 50090-2006) [23], the general specifications for design of highway bridges and culverts (JTG D5) [24], and the specifications for the design of highway steel bridges (JTG D64-2015) [25].



(a)



(b)

**Figure 3.** View of the Xi'an Weihe bridge: (a) perspective view; (b) elevation.

The real joint type in the Xi'an Weihe bridge project is the integral joint. This type of structure uses high-strength steel and bolts to connect the braces and chord to the gusset plate. The advantages of this technique relate to the joint's strength and its fatigue behavior due to the absence of eccentricity and the arc transition, which reduces the stress concentration factor [26]. Consequently, this joint type has been used in bridges such as the Dashengguan Yangtze bridge. The Xi'an Weihe bridge is designed in such a way that the brace sections are different for positive and negative bending. Specifically, the positive bending is designed as a brace I section against the rectangular stiffened joint for negative bending. Figure 4 shows a multi-planar joint for use as the integral joint in the Xi'an Weihe bridge.

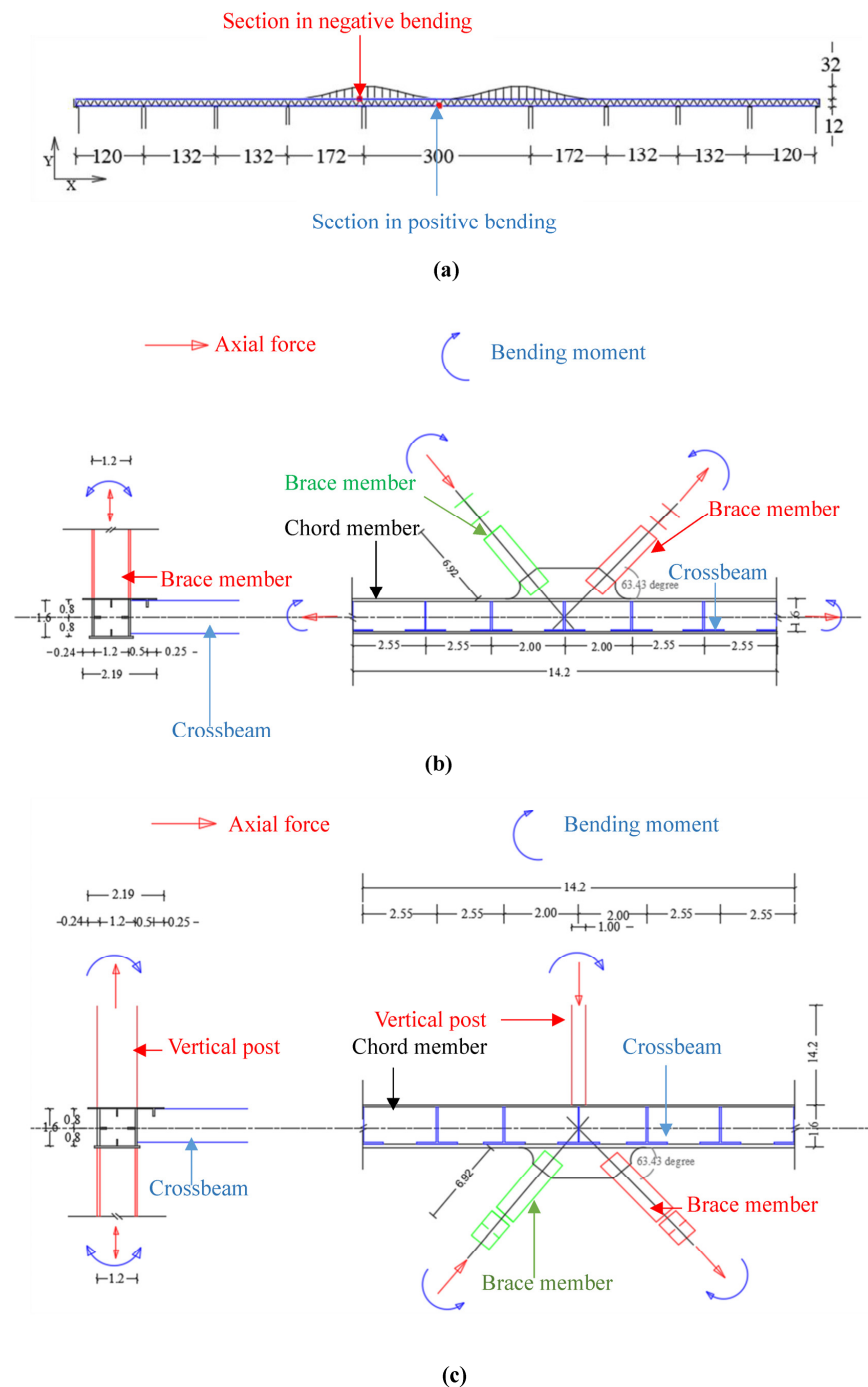


**Figure 4.** Dense-crossbeam structure with the integral joint type: (a) joint positioning; (b) positive bending; (c) negative bending.

The Xi'an Weihe bridge is composed of a Warren truss structure, to which the novel concrete-filled built-up K-joints with different brace sections can be applied. Transversally, the deck system is symmetric along the z-axis. In the present paper, one aspect of the symmetry is considered, taking into account the similarity in the loading and the structure. The dimensions of the novel joint type are set equal to those of the integral joint type, with the implementation of stiffeners in the chord member due to its significant width and height. More precisely, the chord member is a stiffened joint with a height of 1.6 m and width of 1.2 m. For the compression brace, the parameter  $\beta$  is equal to 0.8. This generates a width of 0.96 m, which is taken as the rectangular stiffened section for positive and negative bending. Moreover, the concrete infill inside the chord member is placed along the chord member without a division. In a multi-planar analysis, the crossbeams are considered in the section where, based on the bridge design, the chord member has seven crossbeams, at distances of 2.00 m, 2.55 m, and 2.55 m, multiplied by two for the two sides. A vertical post is considered for the negative bending; it is directly welded to the top chord, with a height of 14.2 m for the real bridge. Figure 5 represents the application of the novel concrete-filled built-up section to the Xi'an Weihe bridge for the two sections (positive bending and negative bending) with all the respective dimensions.

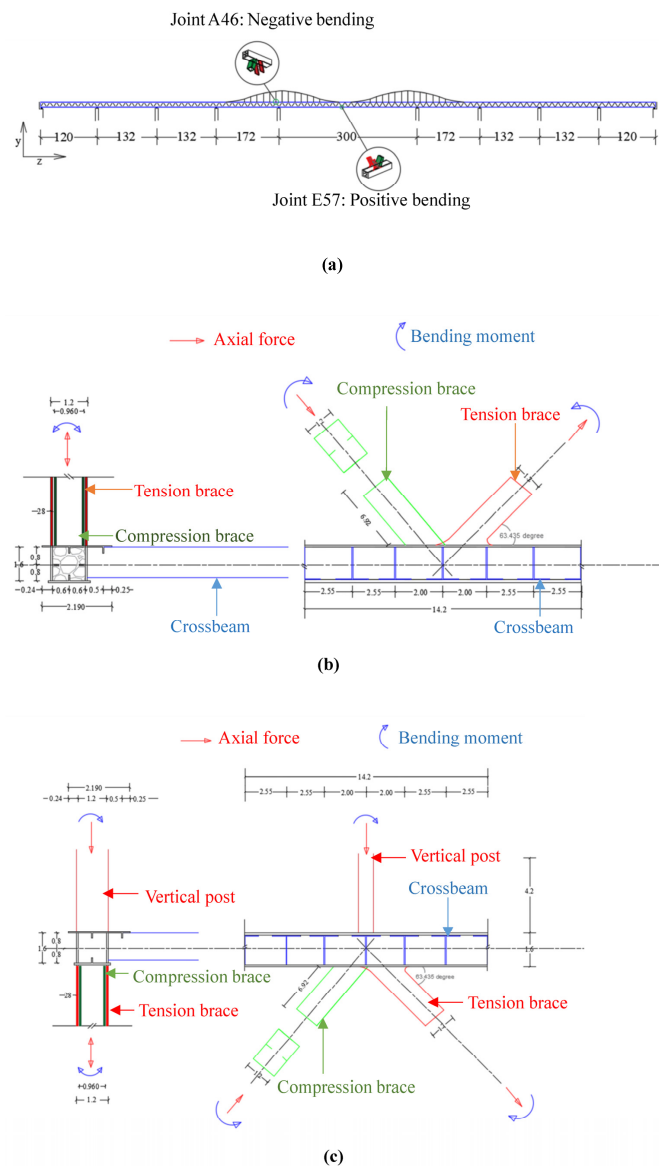


**Figure 5.** Application of the novel joint type in the Xi'an Weihe bridge: (a) joint positioning; (b) positive bending details; (c) negative bending details.

## 2.2. Bridge Structural Analysis

The loadings considered in the analysis are the dead load and the vehicular load. In other words, the wind load, the temperature load, and the climatic load are not included due to their negligible values compared to the first two loadings mentioned. In addition, the sidewalks are neglected due to the fact that their loads are minimal compared to the vehicular load. This assumption presumes that the load transfer is taken through the two trusses of the bridge, which are assumed to be perfectly constructed from manufacture to installation, without any initial defects. Equation (1) represents the load distribution in the truss with the repartition presented in Equation (2):

$$R_i = \frac{n}{R} \Delta_i \quad (1)$$

$$\Delta_i = 1 + \frac{(n+1-2i)6e}{(n^2-1)a} \quad (2)$$

where  $R_i$  is the truss load distribution;  $R$  is the total applied load;  $n$  is the number of trusses, which is equal to 2 in the Xi'an Weihe bridge;  $e$  is the manufacturing and erection eccentricity, which is assumed to be 0; and  $a$  is the distance between the two trusses, which is 30.5 m. It can be deduced that  $R_i = \frac{R}{2}$ , which means that the load is equally transferred in the two trusses for both the self-weight and the live load. Indeed, only one aspect of the symmetry of the deck slab can be considered for analysis, but the result can be transposed to the other part.

Two load combinations are considered in the bridge evaluation as the ultimate limit state (ULS) for the strength analysis and the serviceability limit state (SLS) for the initial stiffness and deflection analysis. The basic equation from the Chinese standard [24] is presented as Equation (3):

$$S_{ud} = \gamma_0 S \left( \sum_{i=1}^m \gamma_{Gi} G_{ik} + \gamma_{Qi} \gamma_L Q_{lk} \right) \quad (3)$$

where  $\gamma_0$  is the structure importance coefficient,  $S$  is the effect action of the load combination,  $\gamma_{Gi}$  is the partial coefficient related to the dead load,  $G_{ik}$  is the bridge dead load,  $\gamma_{Qi}$  is the partial coefficient related to the live load,  $\gamma_L$  is the live load adjustment, and  $Q_{lk}$  is the bridge live load combination. By applying all of the coefficients stipulated in the Chinese standard [25], the related load combination in the ultimate limit state (ULS) can be determined as follows (Equation (4)):

$$S_{ud} = 1.20G + 1.4Q \quad (4)$$

In the serviceability limit state (SLS), after the application of the coefficient (based on the Chinese standard [25]), the load combination is (Equation (5)):

$$S_{fl} = G + Q \quad (5)$$

### 2.2.1. Dead Load Evaluation

The dead load is evaluated from the density of the steel and concrete material (for the novel concrete-filled built-up K-joints with different brace sections). For the steel material, it is taken to be 78.5 kN/m<sup>3</sup>, whereas it is 24.5 kN/m<sup>3</sup> for the concrete material [13].

### 2.2.2. Live Load Evaluation

The live load applied to the bridge is in accordance with the Chinese standard [24]. The vehicular design speed is 80 km/h, which gives a lane width of 3.75 m. That divides the bridge into four lanes in the lower deck and six vehicle lanes in the upper deck, with a remaining area of 0.50 m for each side (Figure 6). The Chinese standard [24] defines the vehicular section as having a uniform lane load of  $q_{lk} = 10.5$  kN/ml and a vehicle

load as presented in Figure 7. In addition, the subway line is subjected to railway loading. According to the Chinese standard [24], the line is spaced to 4.2 m with loading composed of four vehicles with a length of 23.92 m and a load value of 145 kN (Figure 8).

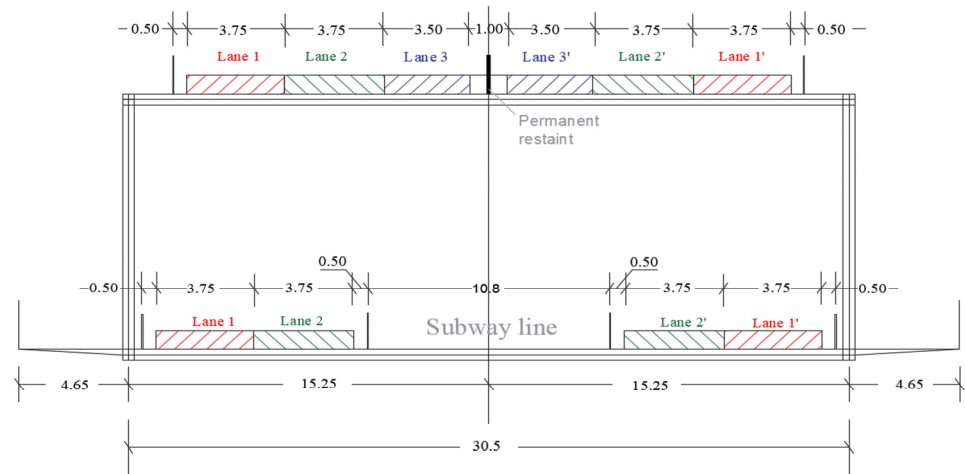


Figure 6. Structure of the Xi'an Weihe bridge lane.

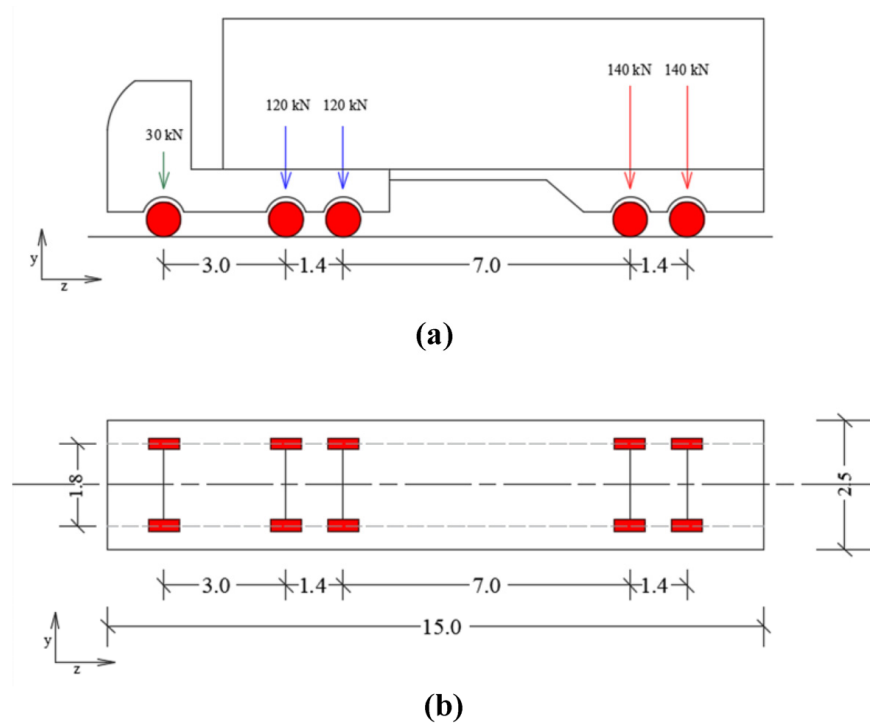


Figure 7. Analysis of the bridge's vehicular load: (a) longitudinal view; (b) plan view.

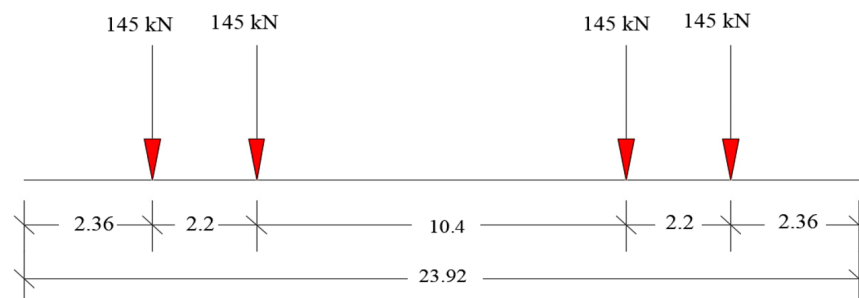


Figure 8. Railway loading in bridge design.

Two sections, comprising the positive bending and negative bending, are considered in the analysis. The former is located at the bridge's mid-span (joint E57 in Figure 9), considering that the bending moment causing deflection is at its maximum in that section. The latter is considered at the support (joint A46 in Figure 9), considering that it is the most desirable aspect of a structure. In this context, a bridge structural analysis is carried out using the MIDAS CIVIL software by introducing the bridge geometry and loadings in accordance with the Chinese standard [25] in order to determine the loading on the chord member, brace member, and crossbeams (Figure 9), the results of which are presented in Tables 1 and 2. The results are known to be accurate because this software has been used in several bridge analyses, from the infrastructure to the superstructure [27–30]. Representations of the loadings in positive bending and negative bending in ULS and SLS, respectively, are represented in Figures 10–13.

**Table 1.** Joint E57: positive bending.

Element		Force (kN)	Moment (kN·m)	Force (kN)	Moment (kN·m)
		Ultimate Limit State		Serviceability Limit State	
Joint	End chord 1	28,613.32	−2249.89	22,799.12	−1706.98
	End chord 2	21,957.71	2023.31	17,735.81	1720.23
	Compression brace	−7396.36	4987.25	−5683.55	3896.25
	Tension brace	7505.84	5213.83	5646.51	4083.00
Crossbeam	Num 1	596.89	−2801.75	430.06	−2124.49
	Num 2	598.21	−2797.65	430.86	−2121.66
	Num 3	425.46	−3070.74	294.52	−2336.04
	Num 4	372.55	−4318.93	286.16	−3312.54
	Num 5	545.91	−2921.58	391.81	−2215.73
	Num 6	702.75	−2632.1	514.87	−1988.9
	Num 7	677.01	−2669.66	493.73	−2019.98

**Table 2.** Joint A46. Negative bending.

Element		Force (kN)	Moment (kN·m)	Force (kN)	Moment (kN·m)
		Ultimate Limit State		Serviceability Limit State	
Joint	End chord 1	24,600.25	−39,698.80	20,066.22	−32,537.56
	End chord 2	69,969.74	−26,133.28	57,101.738	−21,368.15
	Compression brace	−58,825	11,342.50	−47,976.88	9310.03
	Tension brace	42,697.19	−2564.47	34,896.60	−2070.67
Crossbeam	Num 1	369.00	−2052.03	254.39	−1524.99
	Num 2	438.50	−2209.17	311.53	−1655.53
	Num 3	398.61	−2471.81	283.33	−1866.63
	Num 4	440.45	−3819.24	327.84	−2913.22
	Num 5	335.32	−2278.12	248.02	−1703.20
	Num 6	362.76	−2064.56	252.46	−1531.24
	Num 7	374.55	−2055.47	261.71	−1523.96
Vertical post		−14,427.74	22,343.55	−11,701.45	18,408.77

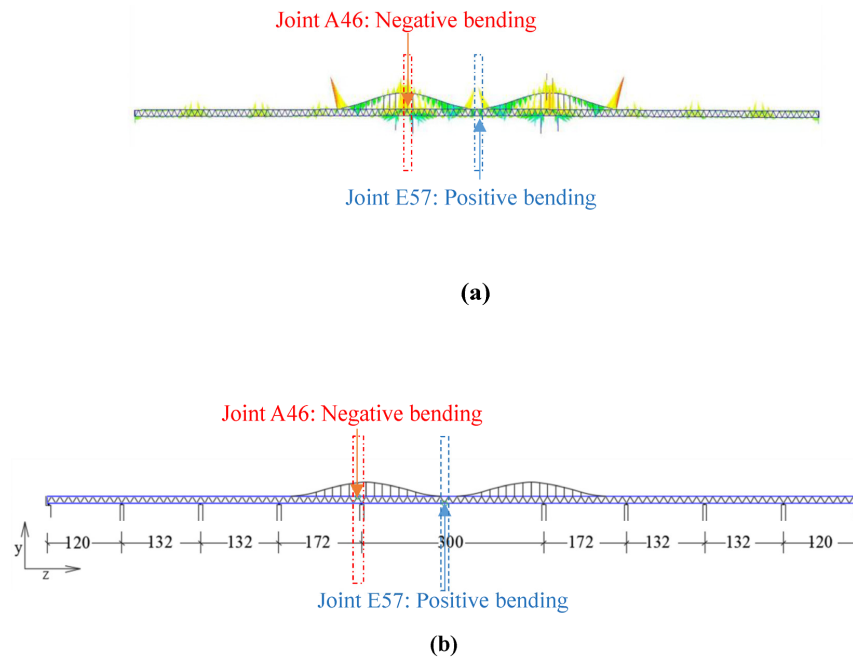


Figure 9. Section for analysis: (a) MIDAS analysis results; (b) analyzed joints.

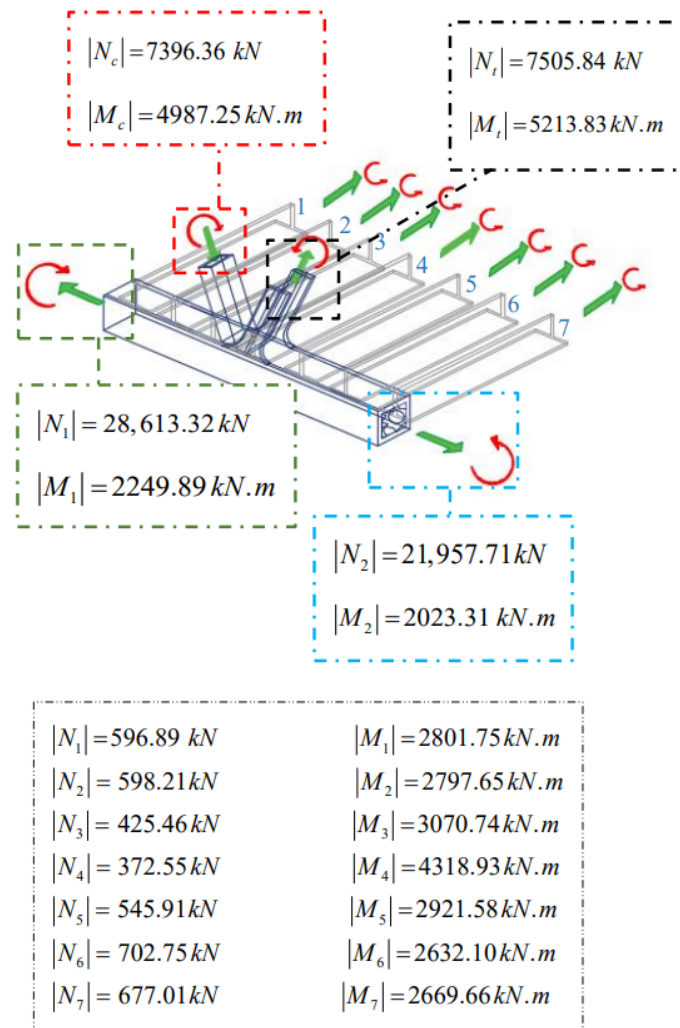


Figure 10. Representation of the applied loading of the Joint E57: positive bending in ULS.

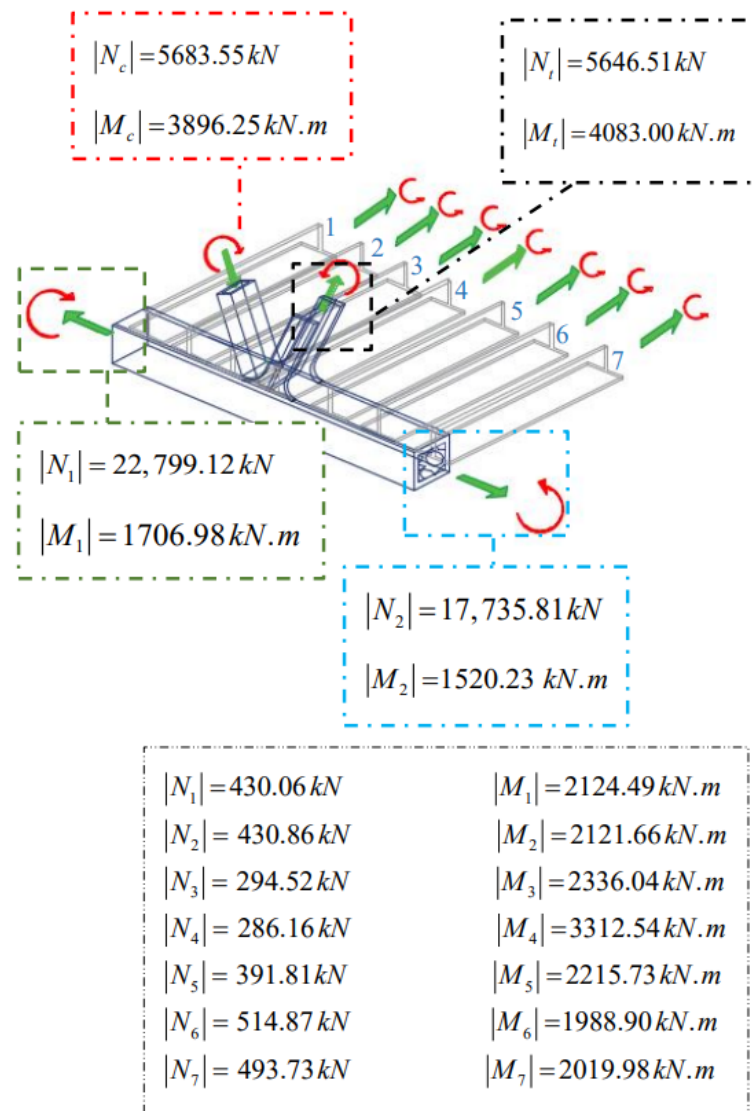


Figure 11. Representation of the applied loading of the Joint E57: positive bending in SLS.

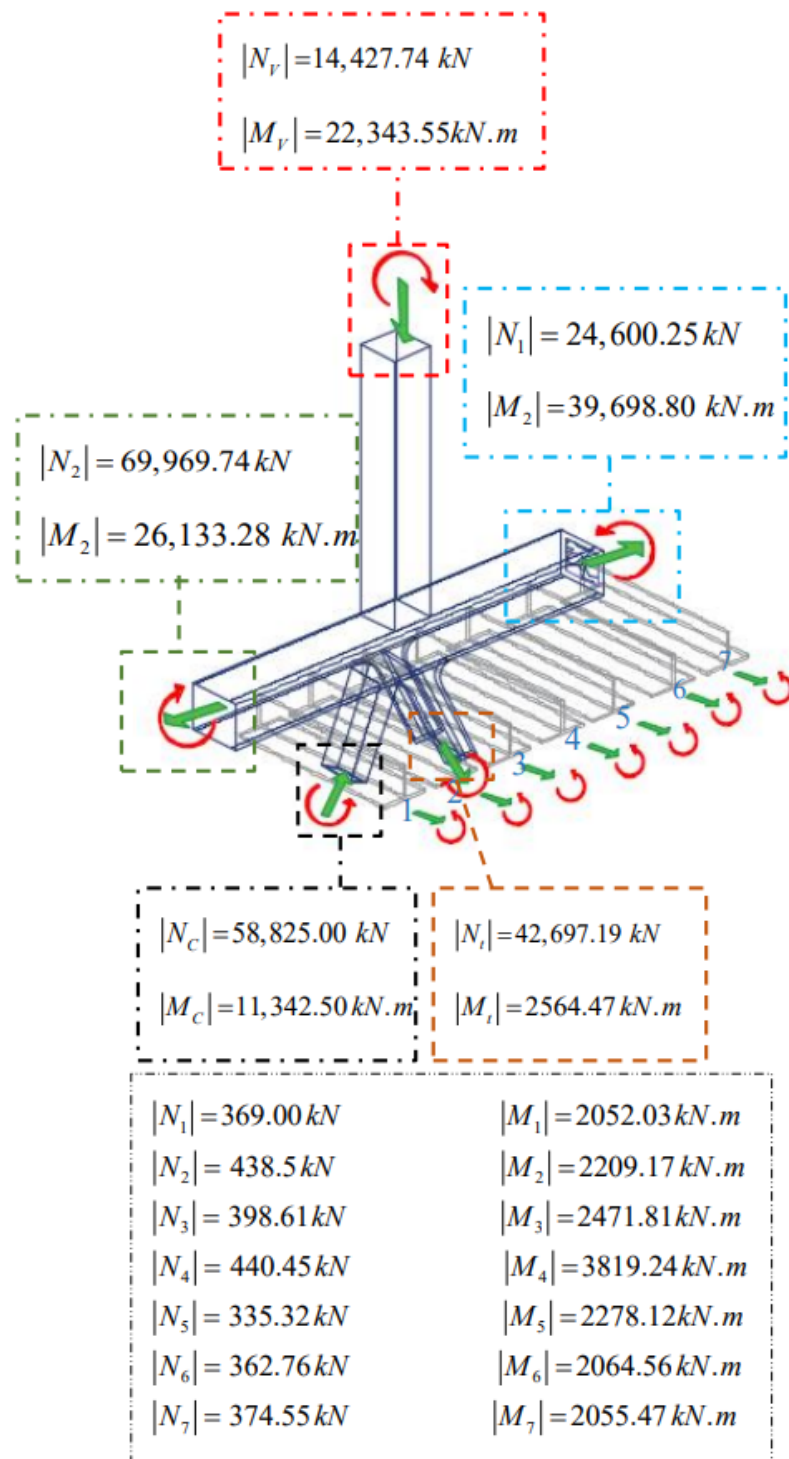
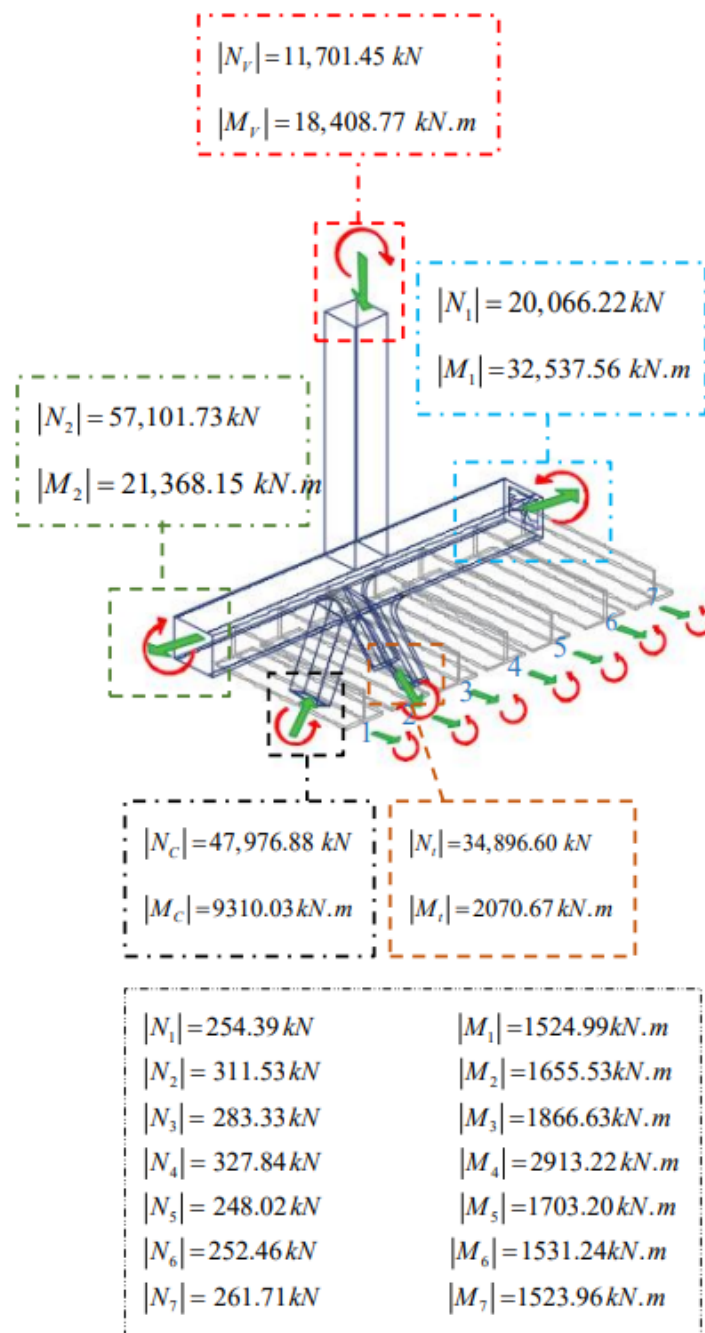


Figure 12. Representation of the applied loading of the Joint A46. Negative bending in ULS.



**Figure 13.** Representation of the applied loading of the Joint A46. Negative bending in SLS.

### 2.3. Numerical Simulation Model

Numerical simulation model analysis is carried out using Abaqus 6.14. Only half of the bridge (one aspect of the symmetry) is considered in the finite element analysis, as it is the focus of the present paper. In the model, the length of the chord member is considered as the mid-point of two consecutive joints, whereas the length of the brace member is set to half of the height of the truss. Regarding the multi-planar element in three dimensions, seven crossbeams are considered in half of the bridge's width, which is 15.25 m (Figure 14).

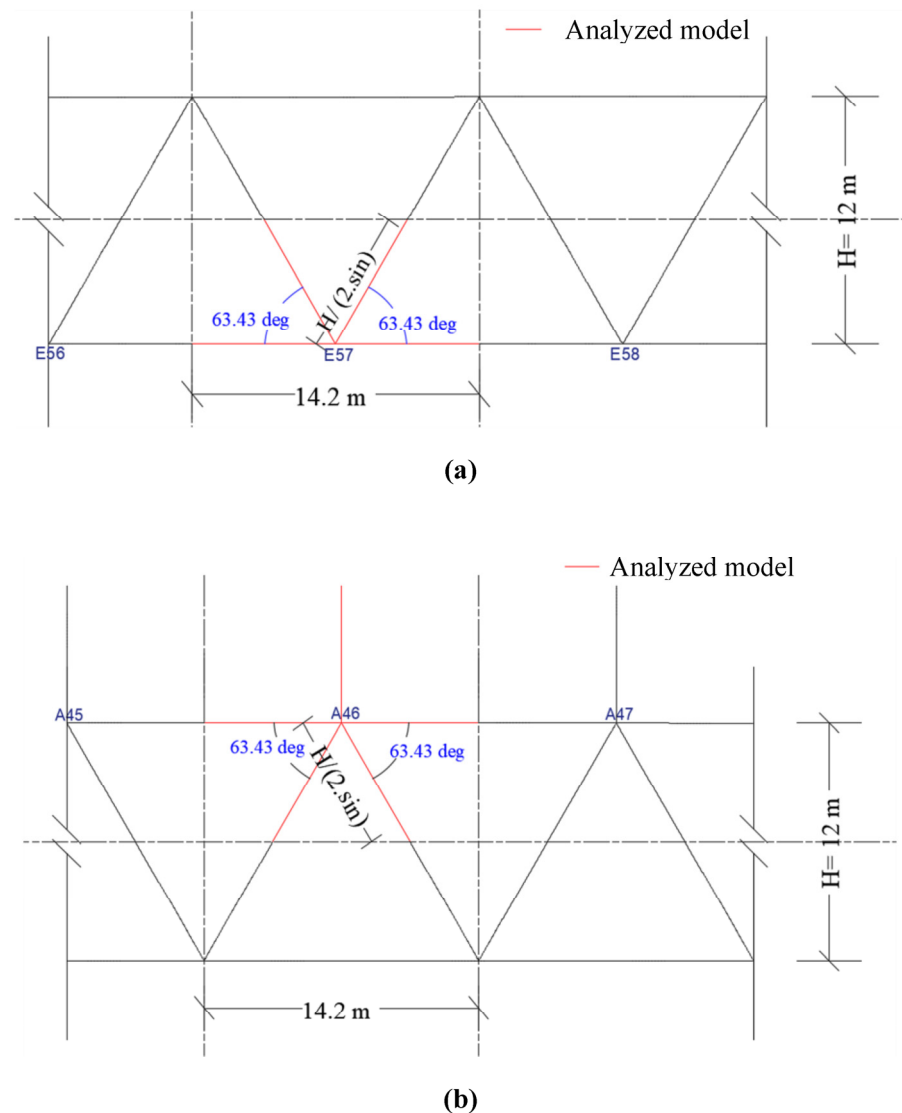


**Figure 14.** Simulated models: (a) positive bending; (b) negative bending.

Assuming that the load is transferred to the chord member through the crossbeams, two types of models are considered, excluding the deck slab and including it, in order to determine its effect on the structure. The considered loadings in the structure are the internal forces in the chord member, the brace members, the crossbeams, and the vertical post (for the negative bending) (Tables 1 and 2). However, the results of the mentioned tables demonstrate that the crossbeams axial forces are less than 3% of the loading in the chord member and the brace member and that these can be neglected. Therefore, it is assumed that the crossbeams are only subjected to bending. In addition to that, taking into account the symmetry of the structure along the  $z$ -axis, the moments at the crossbeams are replaced with their adequate punctual loads multiplied by the length of the element ( $14.05$  m) (Figure 15) (Equation (6)). In that regard, the punctual load for each crossbeam is presented in Tables 3 and 4.

$$P_i = \frac{M_i}{l_c} \quad (6)$$

where  $M_i$  is the adequate moment presented in Tables 1 and 2, and  $l_c$  is the length of the crossbeam.

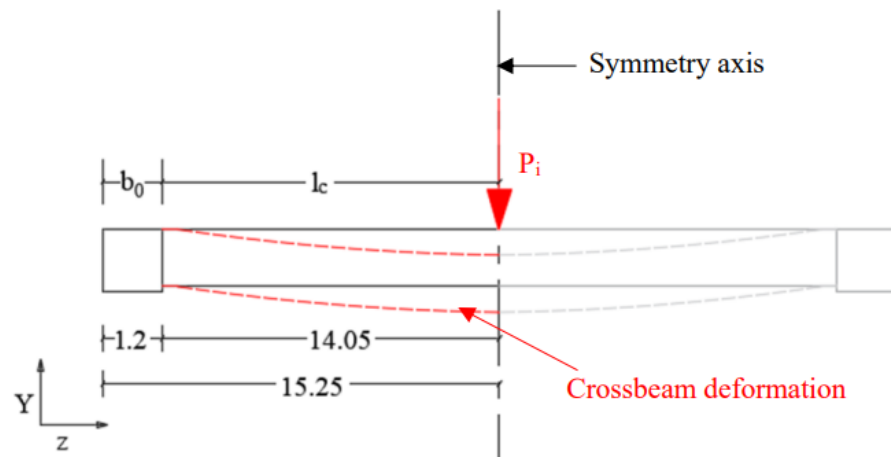


Figure 15. Loading of the crossbeam.

Table 3. Crossbeam applied punctual load: Joint E57—positive bending.

Element	Moment (kN·m) (Result of Structural Analysis)	Applied Loading (kN) $P_i = \frac{M_i}{l_c}$	Moment (kN·m) (Result of Structural Analysis)	Applied Loading $P_i = \frac{M_i}{l_c}$
	Ultimate Limit State		Serviceability Limit State	
Crossbeam	Num 1	−2801.75	−199.41	−2124.49
	Num 2	−2797.65	−199.12	−2121.66
	Num 3	−3070.74	−218.56	−2336.04
	Num 4	−4318.93	−307.40	−3312.54
	Num 5	−2921.58	−207.94	−2215.73
	Num 6	−2632.1	−187.34	−1988.90
	Num 7	−2669.66	−190.01	−2019.98

Table 4. Crossbeam applied punctual load: Joint E57—negative bending.

Element	Moment (kN·m) (Result of Structural Analysis)	Applied Loading (kN) $P_i = \frac{M_i}{l_c}$	Moment (kN·m) (Result of Structural Analysis)	Applied Loading $P_i = \frac{M_i}{l_c}$
	Ultimate Limit State		Serviceability Limit State	
Crossbeam	Num 1	−2050.03	−145.91	−1524.99
	Num 2	−2209.17	−157.24	−1655.53
	Num 3	−2471.81	−175.93	−1866.63
	Num 4	−3819.24	−271.83	−2913.22
	Num 5	−2278.12	−162.14	−1703.20
	Num 6	−2064.56	−146.94	−1531.24
	Num 7	−2055.47	−146.30	−1523.96

In the models, all the steel members composed of the chord member, the brace member, and the crossbeams are merged as one element using the “merge command” to create one part named “steel material”. Therefore, these components are directly in one part in the assembly section. As it is mentioned in the novel type of joint’s introduction, concrete infill is used to retrofit the chord member (Figure 1). The mentioned material is modelled by the “smeared crack model”, as it is a relatively monotonic loading under low confining

pressure. More precisely, it uses an isotropic hardening rule. In that regard, cracks are irrecoverable, so they remain in the rest of the calculation. The concrete infill is in another material, named “concrete”, which interacts with the steel. This interaction has the ability to engage in “normal behaviour: hard contact” and tangential behavior as a “penalty with friction coefficient = 0.25”. The steel material is meshed as “quadratic solid finite elements with reduced integration (C3D20R)” [2] with a mesh value of  $\frac{l_0}{100}$ , whereas the concrete member is meshed in “linear solid finite integration, reduced integration, hourglass control (C3D8R)” [2] with a mesh value of  $\frac{l_0}{50}$ , so as to reduce the overtime analysis. All the thicknesses in the elements are meshed with two layers for a more precise result. Even though these layers have been proven satisfactory for numerical simulation analysis in terms of initial stiffness [1] and ultimate strength [2,13], the present paper carries out result precision analysis through modifying the thicknesses of the layers as two, three, and four layers. Regarding the steel material’s properties, elastic and plastic stages are introduced from the initial step, including the density, the elastic modulus, the yield stress, and the tensile strength. The concrete infill is aimed to retrofit the novel joint in the compression brace. Therefore, its elasto-plastic properties include the density, the elastic modulus, and the compressive strength (Table 5). The related values are taken from the averages of experiments related to the material’s properties conducted by researchers including Kim J.R., et al., Ran Feng et al., and Walter Kenedi [31–33]. Live loads are applied at the loading step via a reference point distributed in the affiliated surface of the chord member, the brace member, and the crossbeam. These are composed of axial forces and bending moments, the values of which are presented in Tables 1–4. Figures 16 and 17 show the numerical model and meshing for the novel joint type and the integral joint, respectively, in relation to positive bending.

**Table 5.** Material properties of the Xi’an Weihe bridge [31–33].

Steel Material				Concrete Material		
Density (kN/m <sup>3</sup> )	$E_s$ (GPa)	$f_y$ (MPa)	$f_u$ (MPa)	Density (kN/m <sup>3</sup> )	$E_s$ (GPa)	$f_{cu}$ (MPa)
78.5	200	350	420	24.5	33.5	45

### 2.3.1. Boundary Condition Analysis

The multi-planar dense-crossbeam system is based on gapped K-joints in a two-dimensional plane along the x-y axis. Along the z-y axis, the symmetric boundary condition in the z direction is set taking into account that only half of the system is modeled. Focusing on the x-y axis, the boundary conditions of the gapped K-joints are analyzed to determine their feasibility in the new multi-planar dense-crossbeams system. For this purpose, our analysis emphasizes the application of the axial loading and the bending in the structure. Specifically, the restraint supports from the boundary condition should allow for the application of the load to procure the adequate deformation. Moreover, the presence of the boundary condition should not interfere the joint deformation following G.J. van der Vegte et al.’s recommendation [34], which stipulates that the chord member length should be six times longer than the chord width. That has been satisfied, as the chord length is equal to 14 m (>7.2 m). In this respect, six types are considered in experiments conducted by other researchers (Figure 18). In most boundary types, some loadings cannot be applied to the structure due to the presence of pin support or fixed support on the chord member or brace member. Only boundary conditions type I and type IV are free in all aspects for the multi-planar dense-crossbeams system, except for the presence of the pin support at one end of the chord, which does not procure the deformation from one axial force. Therefore, the aforementioned axial force is transplanted to the other end of the chord member. This is shown in Figure 19, which presents the type of boundary condition used in the analysis (composed of pin support at one end and roller support at the other end).

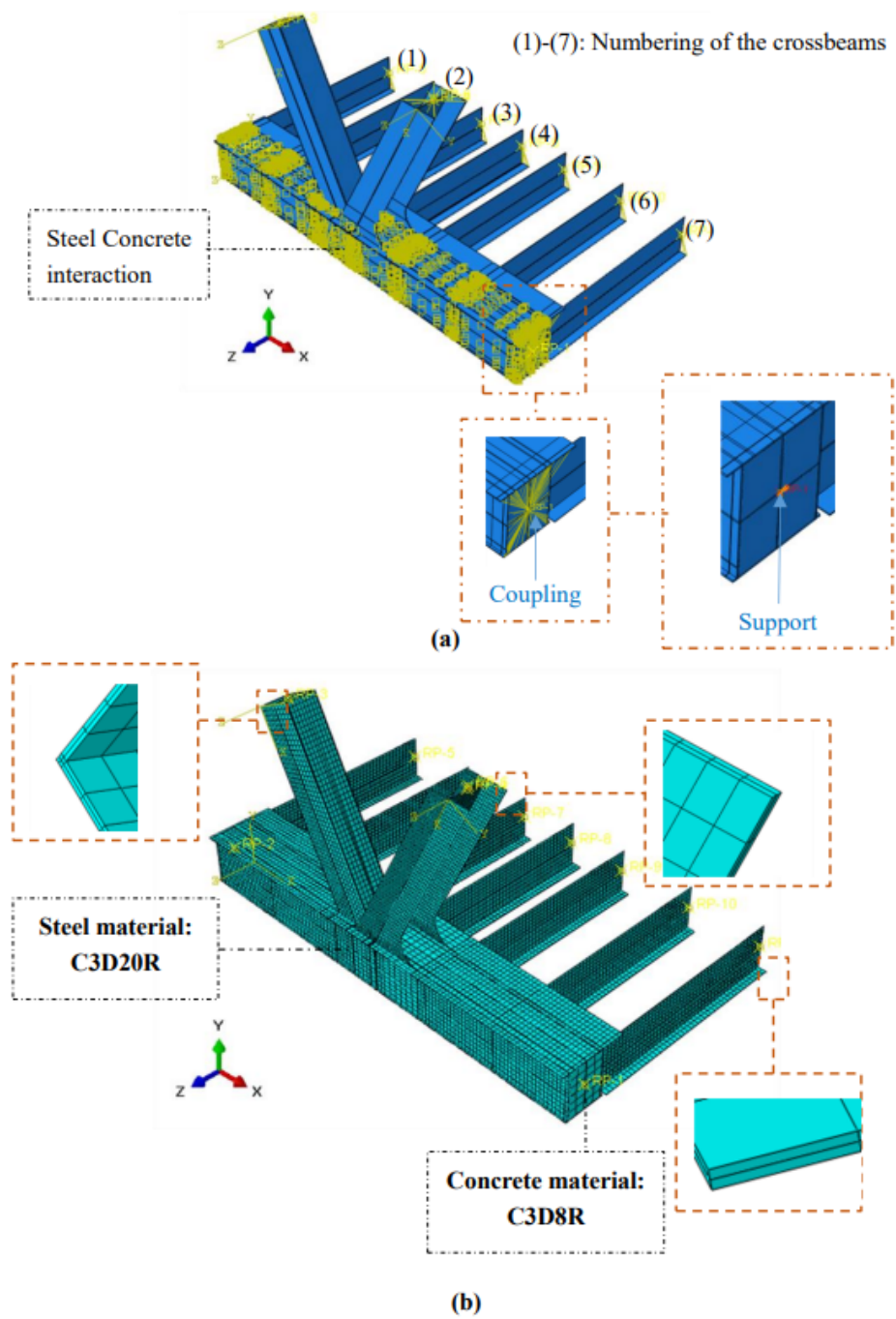


**Figure 16.** Simulation model of the novel concrete-filled built-up K-joints with different brace sections (for positive bending): (a) simulation model; (b) meshing model.

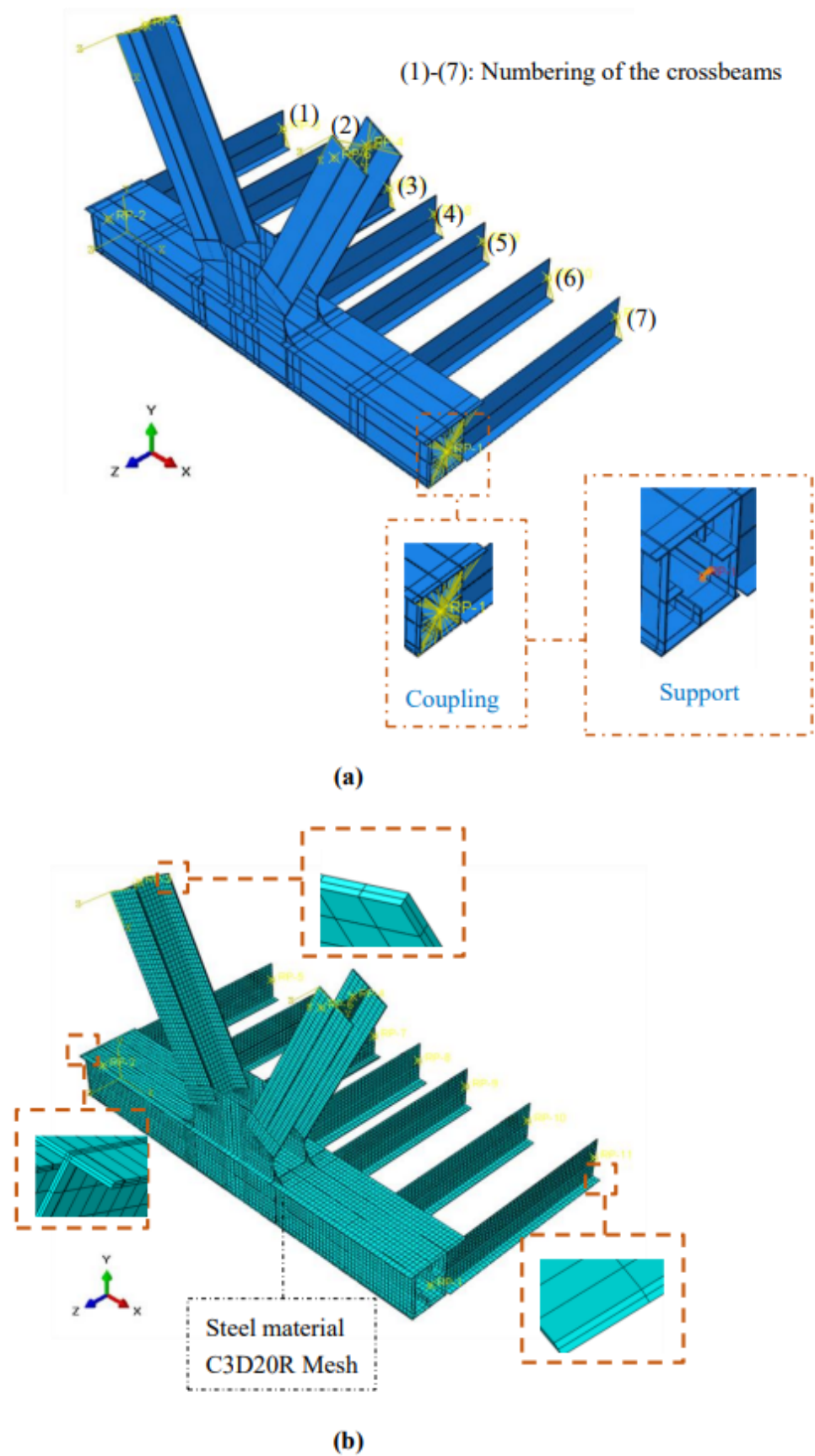
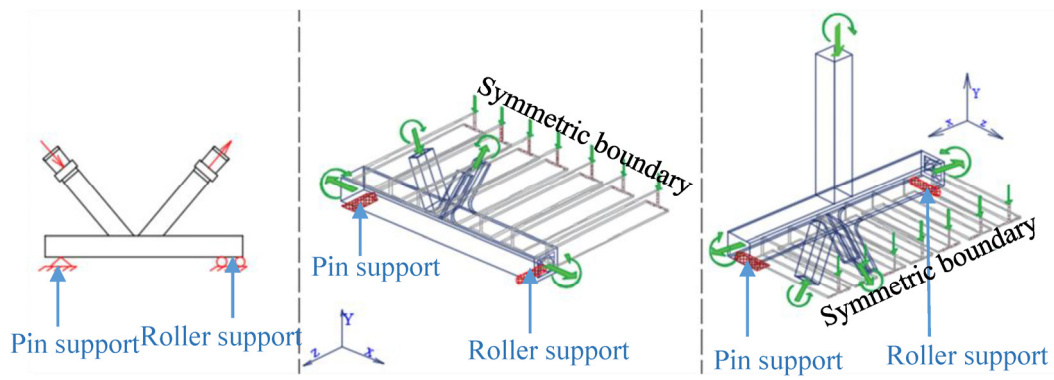
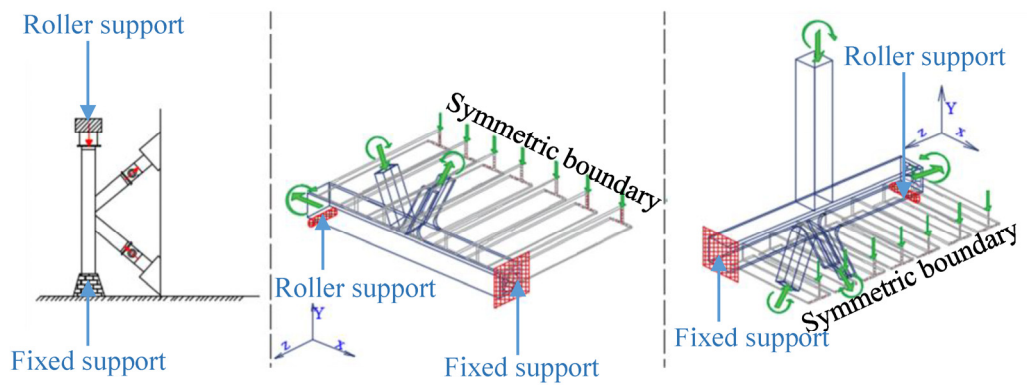


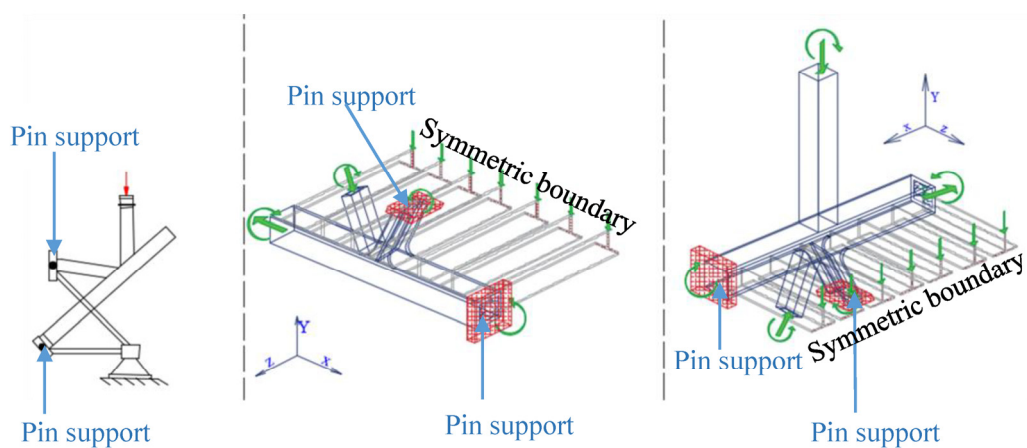
**Figure 17.** Simulation model of the integral joint (for positive bending): (a) simulation model; (b) meshing model.



(a)



(b)



(c)

Figure 18. Cont.

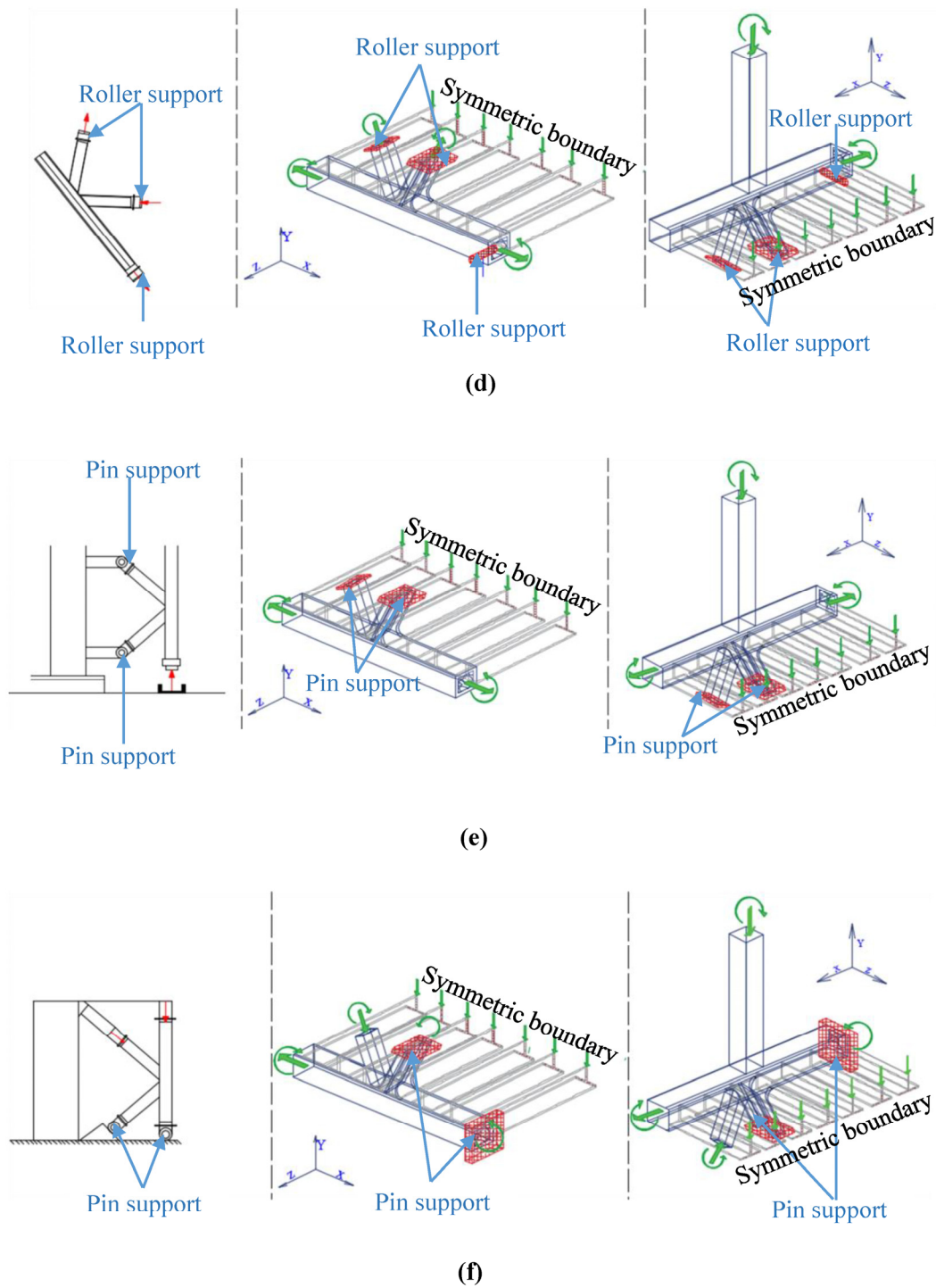


**Figure 18.** Joint boundary conditions and multi-planar applications: (a) ordinary boundary condition type I [2,3]; (b) boundary condition type II [35]; (c) boundary condition type III [31]; (d) boundary condition type IV [32]; (e) boundary condition type V [33]; (f) boundary condition type VI [36].

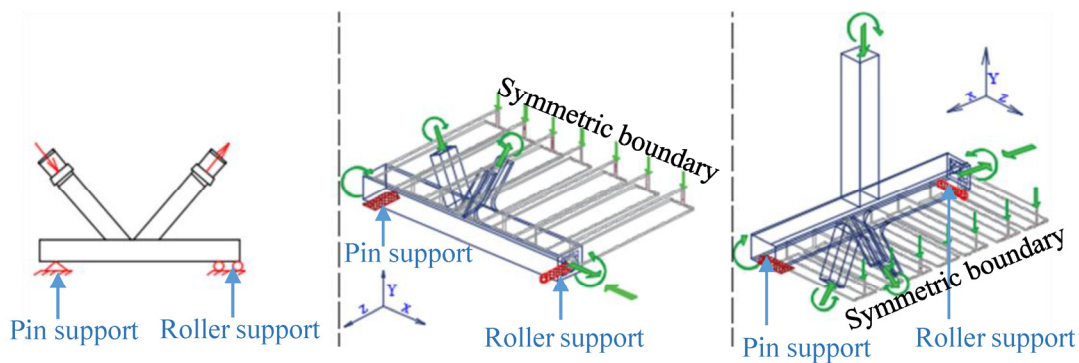


**Figure 19.** Boundary conditions used in the multi-planar analysis.

### 2.3.2. Validation of the Numerical Simulation

As the present paper is the first to apply a multi-planar dense-crossbeam system in engineering, no available experimental data exist that can validate the numerical simulation method. However, this simulation method is similar to the K-gap-joint simulation carried out by other authors, including RHS joints and RCFST joints involving integral joints [13]. The difference in the results is, on average, less than 20% for the initial stiffness and the ultimate strength (Table 6). Additionally, some experiments on Warren truss structures have been conducted that were simulated in the same way; they can therefore be used for verification. The experiments consist of applying loadings at the top mid-span of the truss to create bending. Boundary conditions are a pin support in one chord end and a roller support at the other end. Table 7 shows the parameters related to the truss structure, the material properties of which are presented in Table 8. Table 9 shows the difference in terms of the initial stiffness and deflection, with a difference of less than 20%. The load–displacement curve of the FEM versus experiments that show similarities in the slopes is presented in Figure 20. Therefore, the numerical simulation can be used in the multi-planar truss analysis.

**Table 6.** Joint numerical simulation [13].

Specimen	Type	Initial Stiffness: $K_i$			Ultimate Strength: $U_i$			Ref.
		$K_i$ Exp (kN/mm)	$K_i$ FEM (kN/mm)	Diff (%)	$U_i$ Exp (kN)	$U_i$ FEM (kN)	Diff (%)	
1	KS38-30	981.59	988.98	0.75	156	162.55	4.20	Kim et al. [31]
2	KS38-45	347.26	341.07	1.78	157	155.75	0.80	
3	KS38-60	143.68	113.88	20.74	150	142.35	5.10	
4	KS51-30	2213.57	2397.93	8.33	233	226.63	2.73	
5	KS51-45	326.00	260.23	20.17	187	182.81	2.24	
6	Tc-c11	14.90	17.03	14.31	112.3	117.72	4.83	Liu et al. [37]
7	Tc-c16	11.90	12.33	3.60	103.6	113.72	9.77	
8	Tc-c24	20.29	21.02	3.60	152.9	113.72	25.62	
9	Tc-c28	18.07	19.58	8.34	163	113.72	30.23	
10	Yc-c14	19.56	24.58	25.67	123.2	113.72	7.69	Liu et al. [38]
11	Yc-c16	29.25	22.00	24.79	123.2	113.72	7.69	
12	Yc-c28	40.73	48.47	19.01	186.2	113.72	38.93	

Table 6. Cont.

Specimen	Type	Initial Stiffness: $K_i$			Ultimate Strength: $U_i$			Ref.
		$K_i$ Exp (kN/mm)	$K_i$ FEM (kN/mm)	Diff (%)	$U_i$ Exp (kN)	$U_i$ FEM (kN)	Diff (%)	
13	T-A1	54.63	55.28	1.19	510	483.25	5.25	Bin Cheng et al. [39]
14	T-A2	89.70	101.30	12.93	604	594.94	1.50	
15	T-A3	55.28	62.14	12.42	606	583.26	3.75	
16	T-B1	57.14	57.32	0.30	553	526.78	4.74	Bin Cheng et al. [39]
17	T-B2	146.18	166.67	14.01	655	621.84	5.06	
18	T-B3	82.55	90.70	9.88	680	632	7.06	
19	K0-c14	20.46	23.30	13.84	145	150.583	3.85	Liu et al. [38]
20	k0-c16	21.67	25.78	18.98	109	92.85	14.82	
21	K0-c18	21.69	15.55	28.31	205	165.419	19.31	
22	K2-c18	17.35	19.75	13.81	185	152.232	17.71	
23	k4-c18	18.07	19.20	6.25	172	146.589	14.77	
24	K4-c28	15.67	18.25	16.45	179	152.792	14.64	
25	K1	111.47	90.83	18.52	260	150.88	41.97	Walter [32]
26	K2	238.81	268.78	12.55	224	250.15	11.67	
27	K3	639.55	601.64	5.93	459	504.12	9.83	
28	K4	618.84	700.00	13.11	529	505	4.54	
29	K5	1078.58	1105.47	2.49	815	785.65	3.60	
30	K1C	209.34	240.53	14.90	361	317	12.19	Walter [32]
31	K2C	284.33	273.46	3.83	332	319	3.92	
32	K3C	1102.65	1289.88	16.98	814	892	9.58	
33	K4C	103.45	1125.97	2.04	969	928.45	4.18	
34	K5C	1770.77	1496.06	15.51	1161	985.78	15.09	

Table 7. Truss parameters for verification of the multi-planar truss numerical model.

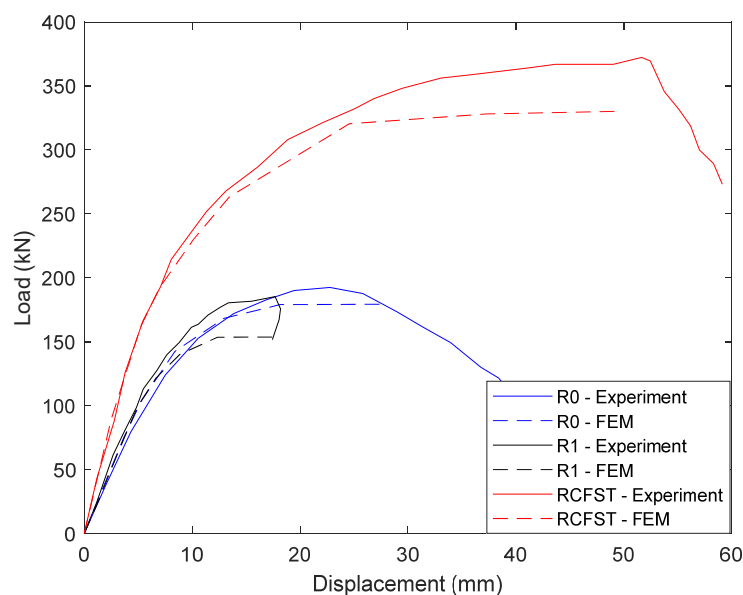
Type	Truss (mm)		Chord Member (mm)								Ref.
	$L_0$	$H_0$	$b_0$	$h_0$	$t_0$	$b_1$	$h_1$	$t_1$	$g$	$\theta$ (deg)	
RHS	3612	625	80	100	3	60	40	3	29	51	Liu et al. [40]
RCFST	3612	625	80	100	3	60	40	3	29	51	
RCFST	4000	880	100	160	3	120	80	3	43	60	Gao et al. et al. [41]

Table 8. Material properties for verification of the multi-planar truss numerical model.

Type	Steel			Concrete		Ref.
	$E_s$ (GPa)	$f_y$ (MPa)	$f_u$ (MPa)	$E_c$ (GPa)	$f_{cu}$ (MPa)	
RHS	200	300	400			Liu et al. [40]
RCFST	200	300	400	34.5	45.9	
RCFST	200	272	-	30	30.4	Gao et al. [41]

**Table 9.** Truss experiments for validation of the numerical simulation.

Type	Initial Stiffness: $K_i$			Load Deflection Limit $f$ (L/360):			Ref.
	$K_i$ Exp (kN/mm)	$K_i$ FEM (kN/mm)	Diff (%)	$\Delta_i$ Exp (kN)	$\Delta_{lim}$ FEM (kN)	Diff (%)	
RHS Truss	18.90	20.60	8.24	123.94	103.47	16.51	Liu et al. [40]
RCFST Truss	21.00	19.36	7.82	143.53	133.79	6.79	Liu et al. [40]
RCFST Truss	31.142	35.782	3.66	250.67	241.0	3.84	Gao et al. [41]



**Figure 20.** Load–displacement curves of the truss experiment versus FEM (Liu Yongjian et al. [40] and Gao Yimin et al. [41]).

**2.4. Result Precision from the Number of Layers in the Thickness**

The precision of the results depending on the layers in the element’s thickness remains controversial. In addition to that, no specific research has addressed this topic. Therefore, differences in the results are analyzed focusing on the joint deformation through modifying the number of layers as two, three, and four. In that regard, the novel multi-planar joint in positive bending (joint A46) is analyzed in the ULS, and the deformations are presented in Figure 21. The adequate results are presented in Table 10, which shows that modification of the number of layers from two to four procures a 0.49 mm difference (relatively negligible). However, there is a need to mention that increasing the number of layers consumes more time in the numerical simulation. Taking into account these parameters, the number of layers in the present paper is set equal to two.

**Table 10.** Results’ precision by modifying the layers in the thickness–joint A46 in positive bending.

	Unit	Thickness in Two Layers (n = 2)	Thickness in Three Layers (n = 3)	Thickness in Three Layers (n = 4)
Multi-planar joint deformation (joint A46)	mm	13.78	13.48	13.29

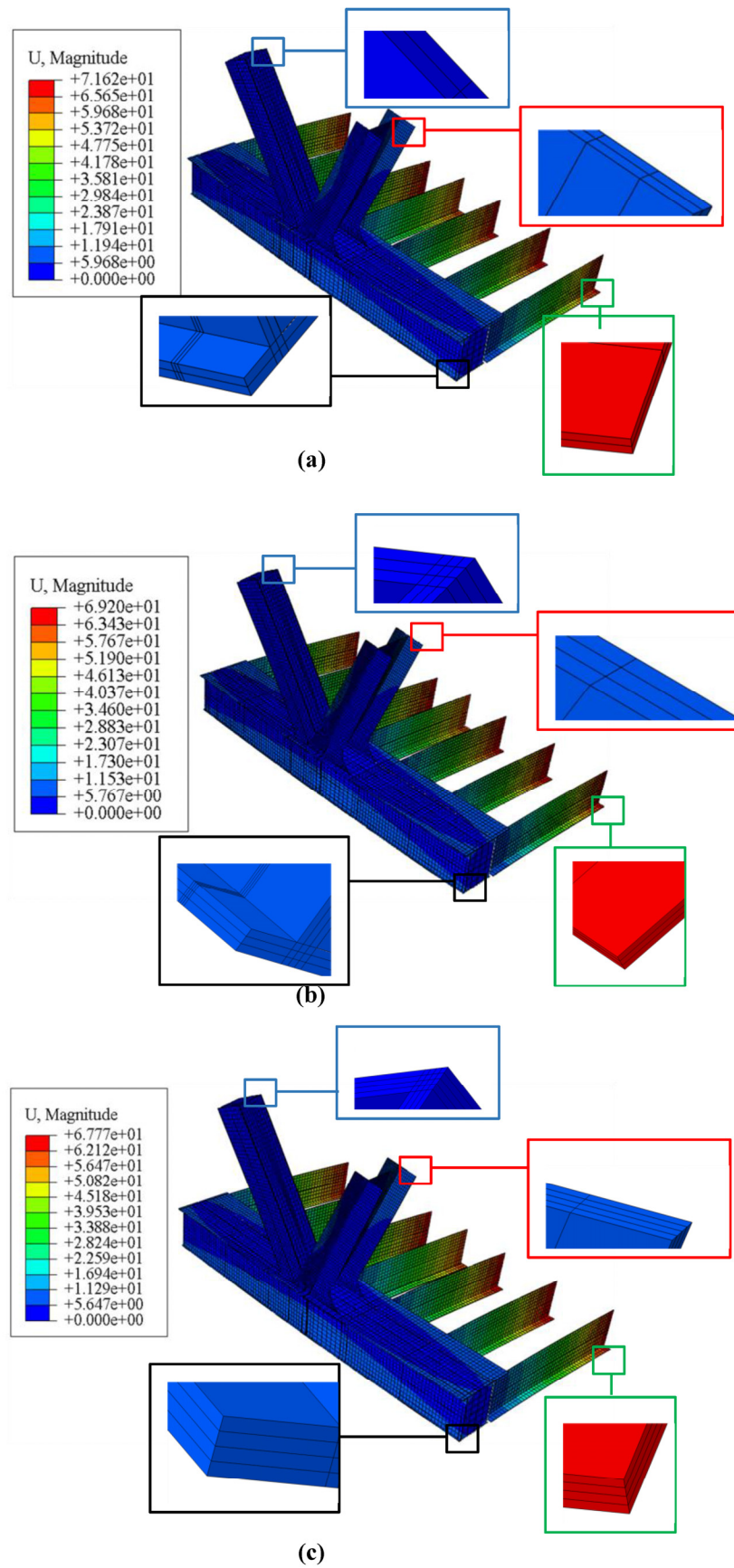


**Figure 21.** Multi-planar joint deformation with different numbers of layers: (a) two layers (mm); (b) three layers (mm); (c) four layers (mm).

### 2.5. Numerical Result of the Strength Verification

As two types of analysis were carried out using the described numerical simulation, the results comprise the multi-planar dense crossbeam deflection with the initial stiffness and the multi-planar dense crossbeam strength.

#### 2.5.1. Determination of Deflection and Initial Stiffness

The determination of the deflection and the initial stiffness was carried out in the serviceability limit state (SLS) according to the Chinese Standard [25], which limits the deflection to  $\frac{l_0}{500}$ .  $l_0$  is the length of the multi-planar dense-crossbeam system and is 14,200 mm. The initial stiffness is determined from Equation (7):

$$K_i = \frac{N}{\Delta} \quad (7)$$

where  $N$  is the maximum loads applied in the SLS and  $\Delta$  is the maximum deflection in the SLS.

Table 11 presents the results of the analysis in the SLS. The results show that the deflection is less than the deflection limit for both the integral joint and the novel concrete-filled built-up K-joint with different brace sections. The percentage of material use ( $P_m$ ) can be also calculated based on the ratio of the deflection to the deflection limit (Equation (8)):

$$P_m = \frac{\Delta}{\Delta_{lim}} \cdot 100 \quad (8)$$

**Table 11.** Serviceability limit state deflection and initial stiffness.

Type of Bending	Structure	Deflection Maximal (mm)	Deflection Limit (mm)	Percentage of Use of Material ( $P_m$ ) (%)	Initial Stiffness ( $\frac{kN}{mm}$ )
Positive bending without deck slab	Novel-type concrete-filled built-up structure with different brace sections	10.21	28.4	35.95	553.04
	Integral joint	13.25	28.4	46.65	426.15
Positive bending with deck slab	Novel-type concrete-filled built-up structure with different brace sections	2.01	28.4	7.08	2809.21
	Integral joint	4.83	28.4	17.01	1169.05
Negative bending without deck slab	Novel-type concrete-filled built-up structure with different brace sections	13.13	28.4	46.23	3653.99
	Integral joint	15.25	28.4	53.70	3146.02
Negative bending with deck slab	Novel-type concrete-filled built-up structure with different brace sections	5.58	28.4	19.65	8598.01
	Integral joint	7.68	28.4	27.04	6246.99

#### - Comparison of the joint systems

For positive bending, the novel joint type has a maximum deformation of 10.21 mm, compared to 13.25 mm for the integral joint when the slab is excluded (Figure 22). From this, the difference in the percentage of material use ( $P_m$ ) can be determined to be 10.70%. When including the deck slab, the novel joint type has a maximum deflection of 2.01 mm, compared to 4.83 mm for the integral joint (Figure 23). This means a difference in the percentage of material use ( $P_m$ ) of 9.93%. These results confirm the strength of the novel joint type as compared to the integral joint type due to the existence of the concrete infill,

which has higher compressive strength [2] and bending strength [42] than the hollow-section joint.

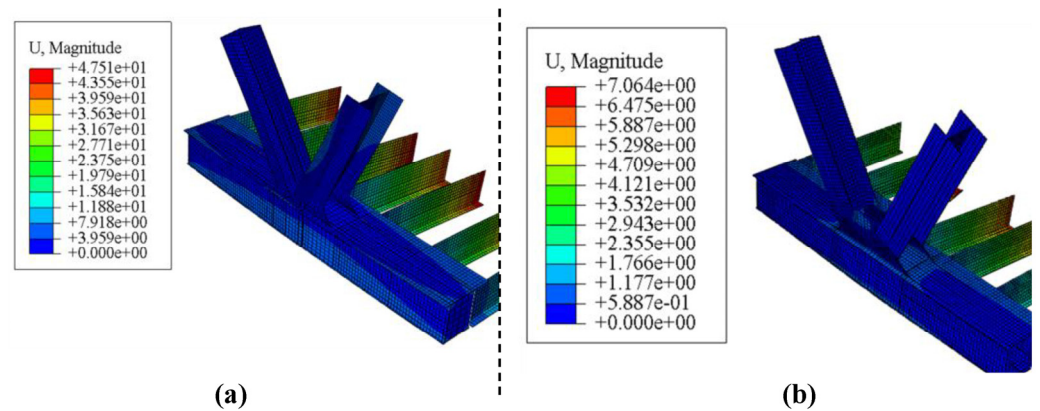


**Figure 22.** SLS deformation under positive bending without a deck slab (mm): (a) novel concrete-filled built-up K-joint with different brace sections; (b) integral joint.

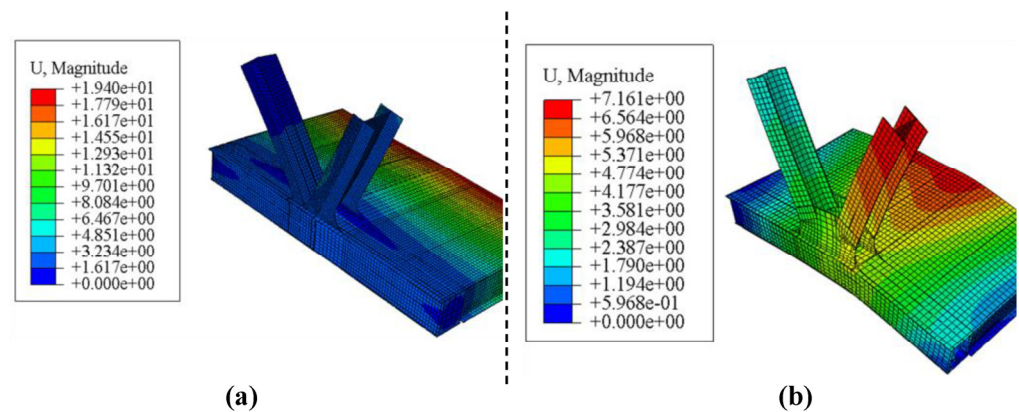


**Figure 23.** SLS deformation under positive bending with a deck slab (mm): (a) novel concrete-filled built-up K-joint with different brace sections; (b) integral joint.

In the negative bending analysis, when the deck slab is excluded, the novel joint type has a maximum deflection of 13.13 mm, compared to 15.25 mm for the integral joint (Figure 24). In terms of the percentage of material use ( $P_m$ ), the novel joint type's deflection is about 46.23%, as compared to 53.70% for the integral joint. Therefore, the difference is 7.46%. When the deck slab is introduced, the novel joint type has a maximum deflection of 5.58 mm, whereas the integral joint has a deflection of 7.68 mm (Figure 25), with values for the percentage of material use ( $P_m$ ) of 19.65% and 27.04%, respectively. This equals a difference of 7.39%, with higher strength being exhibited by the novel type of concrete-filled built-up K-joints with different brace sections due to the concrete infill's compressive [2] and torsional strength [42].

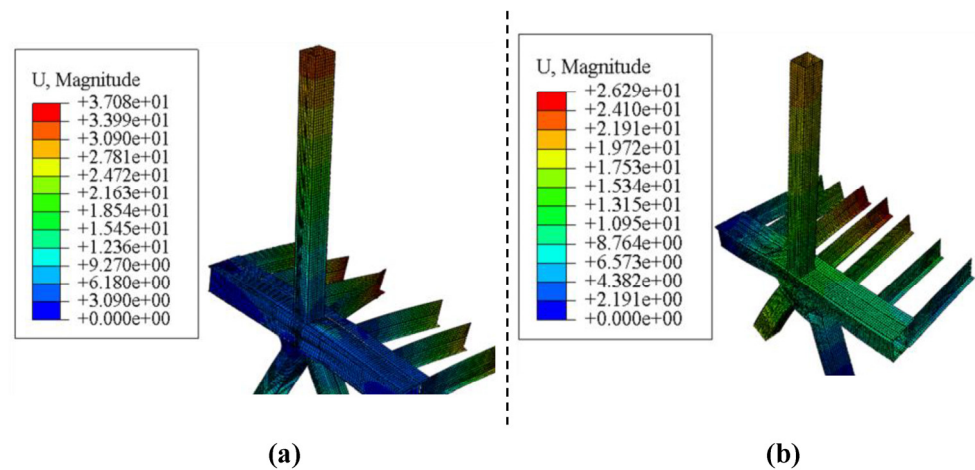


**Figure 24.** SLS deformation under negative bending without a deck slab: (a) novel concrete-filled built-up K-joint with different brace sections; (b) integral joint.

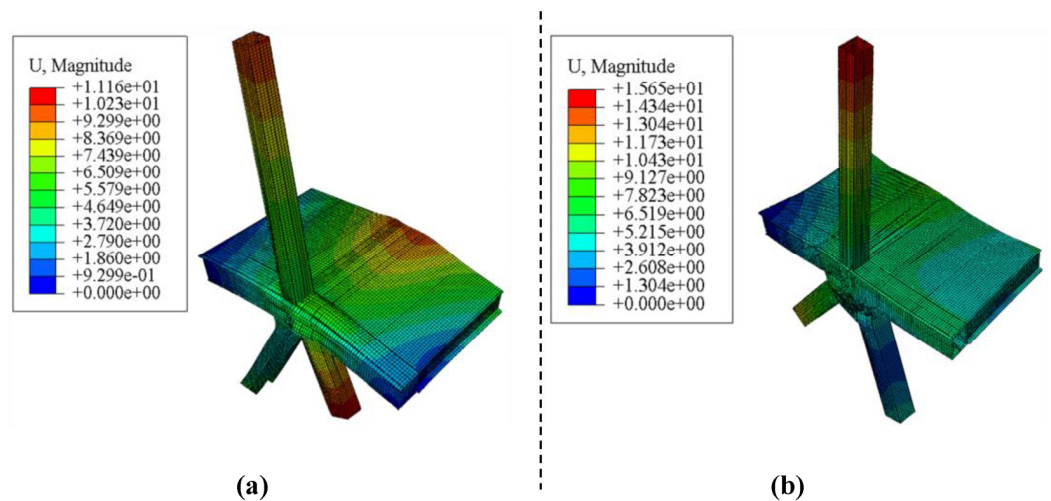


**Figure 25.** SLS deformation under negative bending with a deck slab: (a) novel concrete-filled built-up K-joint with different brace sections; (b) integral joint.

- Effect of the deck slab in the Serviceability Limit State analysis

An analysis of the deck slab is carried out by comparing the same type of system when including and excluding the material (steel deck). In this regard, for the novel joint type under positive bending, the percentages of the use of material ( $P_m$ ) are 35.95% and 7.08% when the deck slab is excluded and included, respectively. This produces a difference of 28.87%, where including the deck slab makes the material stronger. For the integral joint, the percentage of use of material ( $P_m$ ) is 46.65% when the deck slab is not included, as compared to 17.01% when the deck slab is included. Comparing the results gives a difference of 29.64%, to which the deck slab contributes stabilization.

For negative bending, the novel joint shows a maximum deflection of 13.13 mm when excluding the deck slab and 5.58 mm when including it; this gives percentages of use of material ( $P_m$ ) of 46.23% and 19.65%, respectively. The difference in these values is about 26.58%, where the simulation that includes the deck slab results in a higher strength than the simulation that excludes it. For the integral joint, the percentages of use of material ( $P_m$ ) are 53.70% and 27.04% when excluding the deck slab and including it, respectively. This gives a difference of 26.65%, where including the deck slab uses less material.

### 2.5.2. Checking the Ultimate Limit State (ULS)

The verification of the ULS is related to the structure's ultimate strength. According to the CIDECT standard [7], excessive deformation of more than 3% of the chord width produces failure. In other words, the ultimate strength verification is carried out in such a way as to compare the maximal deformation in the ultimate limit state to  $3\%b_0 = 0.03 \times 1200 \text{ mm} = 36 \text{ mm}$  for the case of the Xi'an Weihe bridge. As was the case for the deflection assessment, one numerical simulation is conducted for each of the following scenarios: positive bending and negative bending including and excluding the deck slab. The maximum deformation in the ULS and the percentage of the use of material ( $P_m$ ) in the deformation limit ratio are presented in Table 12.

**Table 12.** Ultimate limit state deformation and percentage of use of material.

Type of Bending	Type of Structure	Deformation Maximum (mm)	Deformation Limit (mm)	Percentage of Use of Material ( $P_m$ ) (%)
Positive bending without deck slab	Novel-type concrete-filled built-up structure with different brace sections	13.78	36	38.28
	Integral joint	20.15	36	55.97
Positive bending with deck slab	Novel-type concrete-filled built-up structure with different brace sections	10.43	36	28.97
	Integral joint	16.59	36	46.08
Negative bending without deck slab	Novel-type concrete-filled built-up structure with different brace sections	19.25	36	53.47
	Integral joint	20.23	36	56.19
Negative bending with deck slab	Novel-type concrete-filled built-up structure with different brace sections	15.98	36	44.14
	Integral joint	16.82	36	46.72

#### - Comparison of the joint systems

The first comparison considers positive bending when excluding the deck slab. The results show that the novel-type concrete-filled built-up K-joints with different brace sections has a maximum deflection of 13.78 mm, compared to 20.15 mm for the integral joint (Figure 26). In relation to the deflection limit, which is 36 mm, the percentages of use of material ( $P_m$ ) are 38.28% and 55.97%. These values produce a difference of 17.69%, with greater strength exhibited by the novel joint type. When the deck slab is included, the novel joint type has a maximum deflection of 10.43 mm, compared to a value of 16.59 mm for the integral type of joint (Figure 27). These values correspond to percentages of use of material ( $P_m$ ) of 28.97% and 46.08%, respectively. The difference in these percentages is 17.11%, with higher strength exhibited by the novel type of concrete-filled built-up K-joints with different brace sections in relation to the maximum deflection compared to the integral joint. This is because the strength of the concrete-filled joint under compression loading [2] and torsional loading [42] is higher than that of the hollow-section joint.

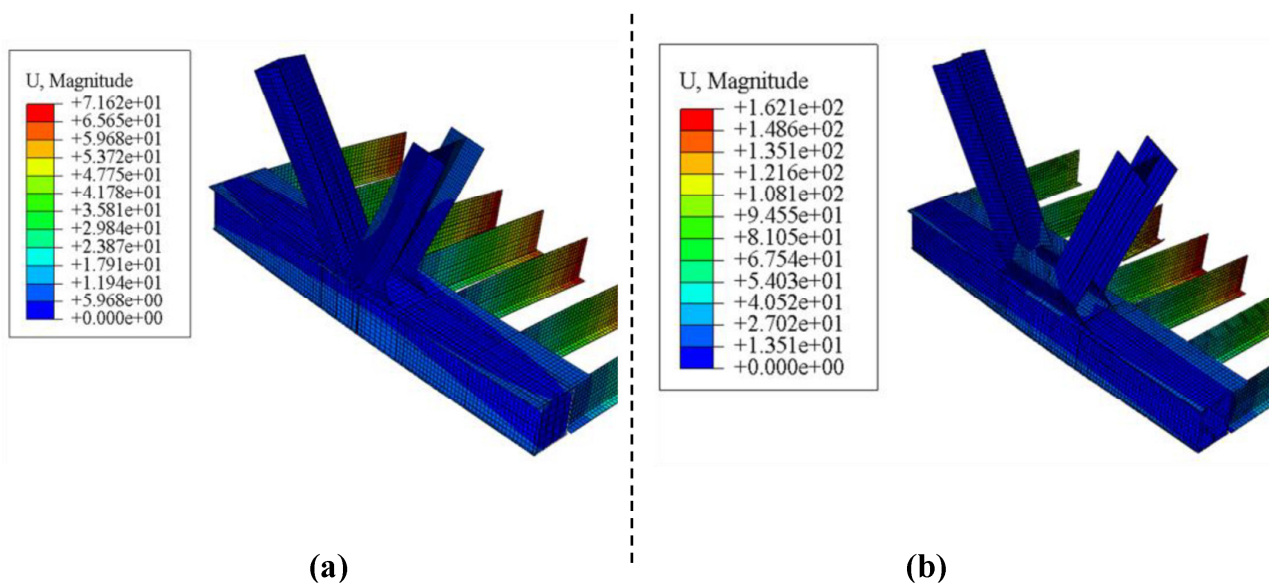


**Figure 26.** ULS deformation under positive bending without a deck slab: (a) novel concrete-filled built-up K-joint with different brace sections; (b) integral joint.

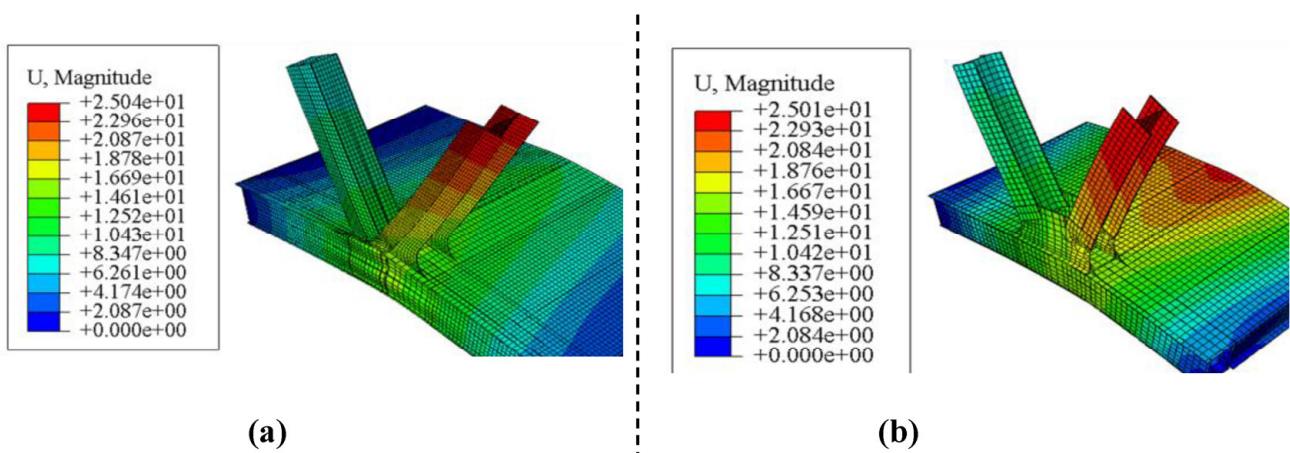


**Figure 27.** ULS deformation under positive bending with a deck slab: (a) novel concrete-filled built-up K-joint with different brace sections; (b) integral joint.

In the negative bending, when excluding the deck slab from the simulation, the novel type of concrete-filled box-section K-joints with different brace sections has a maximum deflection of 19.25 mm, whereas the integral joint has a value of 20.23 mm (Figure 28). This means that the novel joint type has higher strength compared to the integral joint; moreover, the results suggest that the percentages of use of material are 53.47% and 56.19%, respectively. The difference between these two percentages is 2.72%. When including the deck slab in the simulation, the novel type of concrete-filled built-up K-joints with different brace sections has a maximum deflection of 15.89 mm, while the integral joint has a maximum deflection of 16.82 mm (Figure 29). Compared to the deformation limit (36 mm), the percentages of the use of material are 44.14% and 46.72%, respectively, meaning that the novel joint type is stronger (with a 2.58% difference). This difference is due to the compressive strength of the concrete-filled joint [2], along with its torsional strength [42].

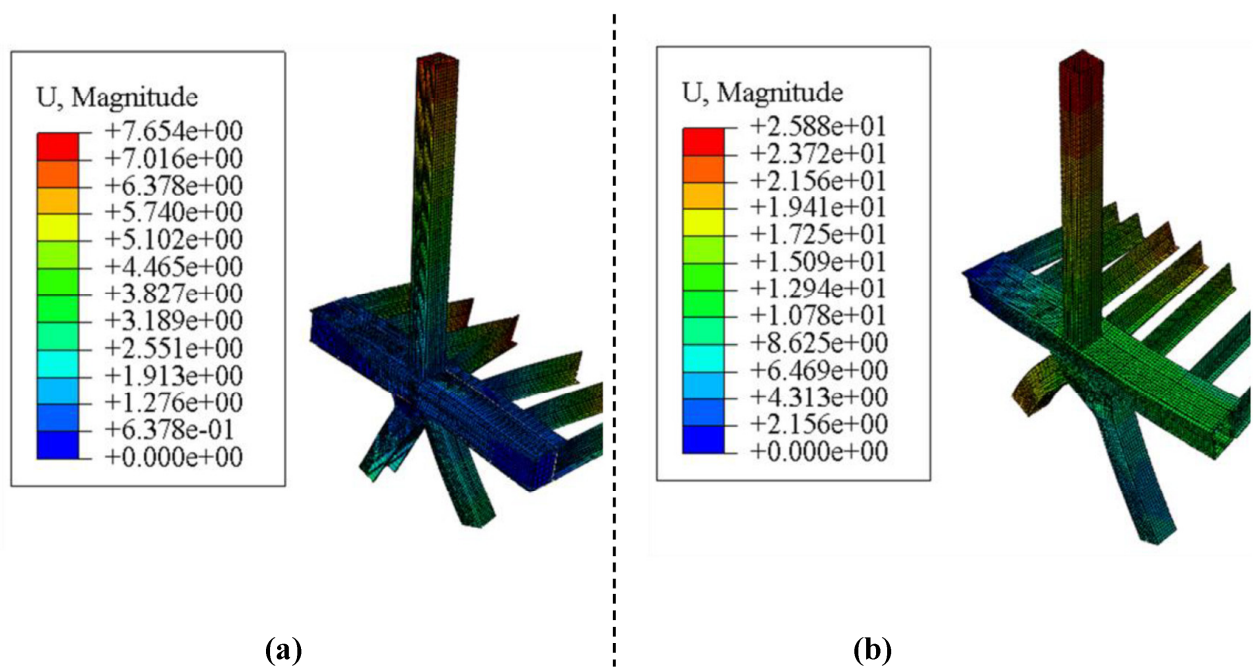


**Figure 28.** ULS deformation under negative bending without a deck slab: (a) novel concrete-filled built-up K-joint with different brace sections; (b) integral joint.

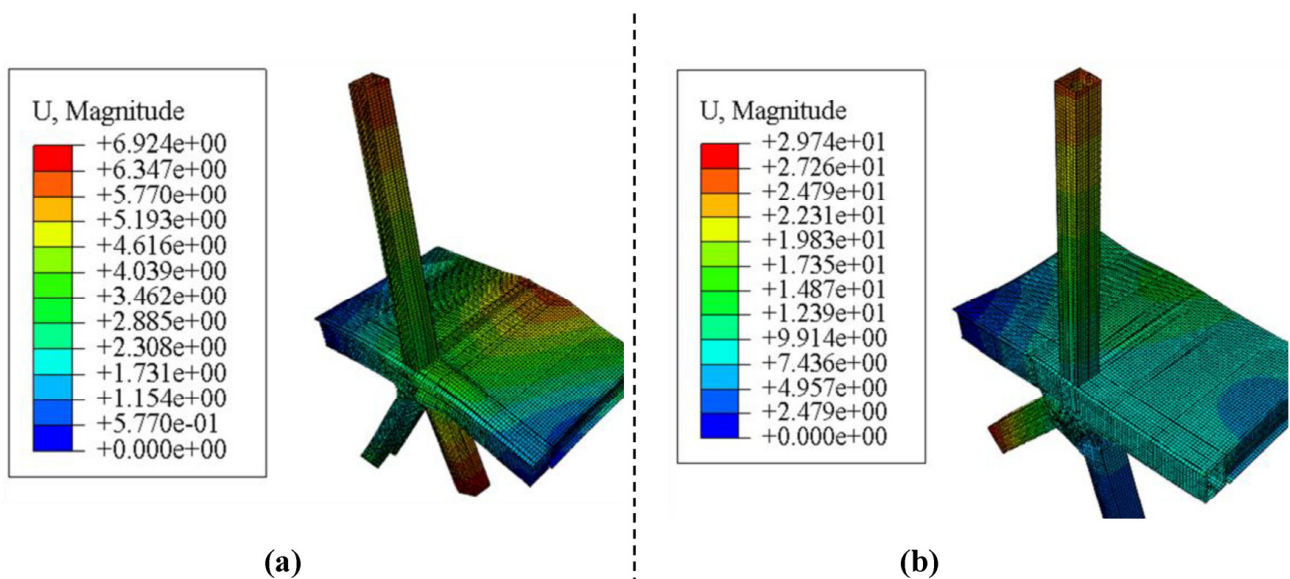


**Figure 29.** ULS deformation under negative bending with a deck slab: (a) novel concrete-filled built-up K-joint with different brace sections; (b) integral joint.

- Effect of the deck slab in Ultimate Limit State analysis

For positive bending, for the novel type concrete-filled built-up K-joints with different brace sections, the percentage of the use of material is 38.28% when excluding the deck slab and 28.97% when the deck slab is included. From these percentages, it can be determined that there is a difference of 9.31%, with the model with the deck slab being stronger. This means that the numerical simulation with the deck slab shows less deformation, meaning that it is more resistant to the loading. For the integral joint, the percentage of the use of material is 20.15% when excluding the deck slab and 16.59% when including it. The difference in the two values is 9.89%, showing that the deck slab contributes to the stabilization of the structure.

For negative bending, the novel concrete-filled built-up K-joints with different brace sections has a deck slab effect of 9.33% in terms of displacement, where including the deck slab produces less deformation. This value is obtained by comparing the percentages of use of material ( $P_m$ ), which are 19.25% and 15.89%, respectively, when excluding and including the deck slab. For the integral joint, the deck slab has an effect of 9.47% on the result of percentage of use of material ( $P_m$ ) related to the deformation when excluding the deck slab (20.23%) and when including the deck slab (16.82%). It can be inferred from the results that the deck slab contributes to stabilizing the structure by reducing the deformation, which is the case in the simulations described in the present paper.

### 3. Failure Analysis of Multi-Planar Dense Crossbeams

In a truss bridge structure, the failure mode is divided into two types, namely, truss failure and joint failure. Truss failure appears in the chord member without interfering with the brace members. In other words, it involves failure outside the joint. This can manifest by bending failure or torsion failure due to the presence of the intermediate crossbeams. Joint failure is characterized by a buckling at the intersection of the chord member to the brace members. It can manifest through chord flange failure, brace failure, and sidewall failure [2]. These phenomena can appear in both novel concrete-filled built-up K-joints with different brace sections and in integral joints. Nevertheless, some types of joint failure cannot appear in the novel joint type due to its behaviors. First, the existence of the concrete infill strengthens the chord member, preventing both the plastification of the chord face and the failure of the chord side wall. Moreover, the arc transition prevents punching shear failure. Finally, the uneven brace section prevents the shear yielding of the chord member. Therefore, the buckling of the compression brace or the buckling of the arc transition are the possible joint failure modes for this type of joint (Figure 30). For the case of the integral joint system, an overview of its failure modes reveals that the plastification of the chord face does not appear to be likely because the brace members are not linked to the chord member; the same is true for punching shear failure and brace failure due to the existence of the gusset plate. Consequently, only the failure of the chord side wall and the buckling of the gusset plate are possible for the integral joint (Figure 31).

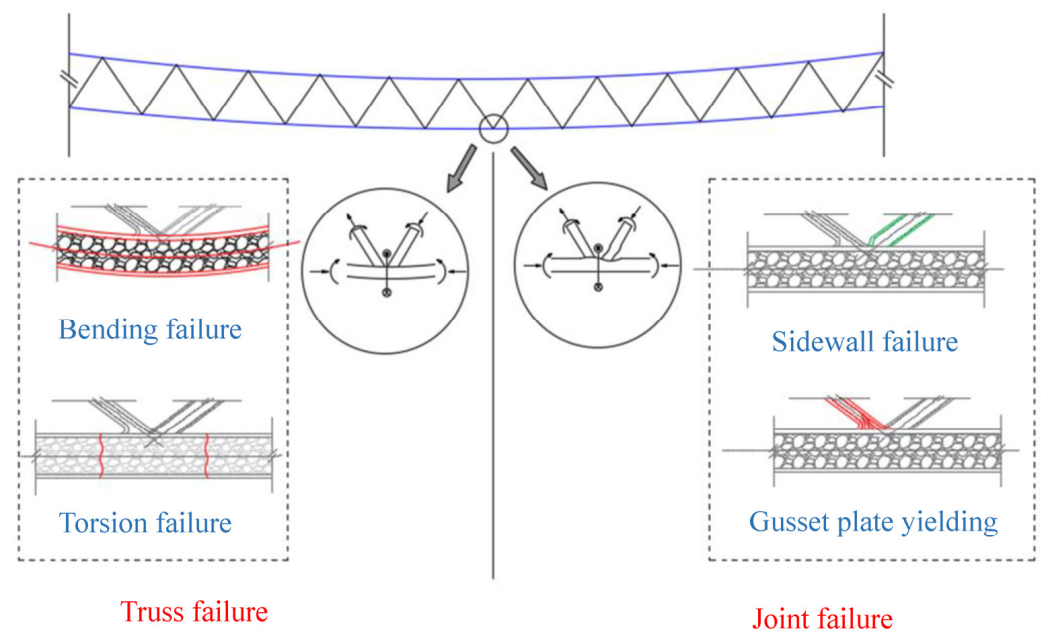


**Figure 30.** Truss-type novel concrete-filled built-up K-joint with different brace sections: failure modes.

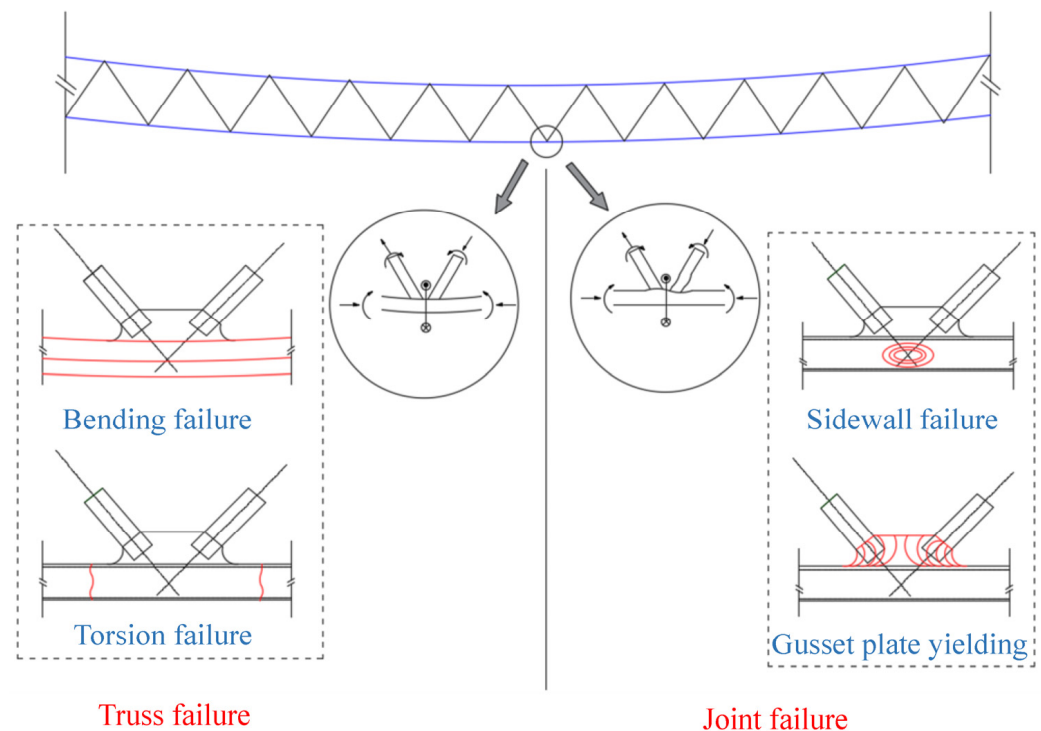


**Figure 31.** Truss-type integral joint: failure modes.

An analysis of the failure mode is carried out for both the novel joint type and the integral joint. Numerical simulation is the method of this investigation, in which precise finite element models (FEMs) are built as a means of verifying the Xi'an Weihe bridge. The methods only differ in terms of the applied loading; the compression and tension loads are increased until the failure of the system. As the numerical simulation with the deck slab is more realistic in relation to this bridge, this model is used to verify the multi-planar ultimate capacity.

### 3.1. Novel Concrete-Filled Built-Up K-Joint with Different Brace Sections

The results of the finite element analysis show that the structure fails due to the yielding of the tension brace arc transition under both positive and negative bending (Figure 32). Indeed, the arc transition is the weakest component in the structure. For positive bending, the FEM results show that the multi-planar novel joint type fails with a compression–tension load equal to 30,285.84 kN. Based on the structural analysis results produced using MIDAS CIVIL software, the load applied to the tension brace is 7505.84 kN in the ULS (Table 1). This generates a percentage of use of material ( $P_m$ ) of 24.78% for positive bending, as compared to the system's ultimate strength. As shown Table 12, we carried out an analysis of the deformation limit ( $P_m$ ) equal to  $0.03b_0$ , which shows a percentage of material use of 28.97%. It can be inferred that there are no significant differences between the two methods (a 4.19% difference).

In terms of negative bending, a tension–compression load of 111,830.25 kN leads to the buckling of the arc transition. The structural analysis showed a loading of 42,697.19 kN for the ULS (Table 2), which is equivalent to 38.18% of the load to failure. Based on the deformation analysis in relation to  $0.03b_0$ , the structure has a percentage of material use ( $P_m$ ) of 44.14%. It can be deduced that the two methods have a difference of around 5.96%, which is acceptable (Table 13).

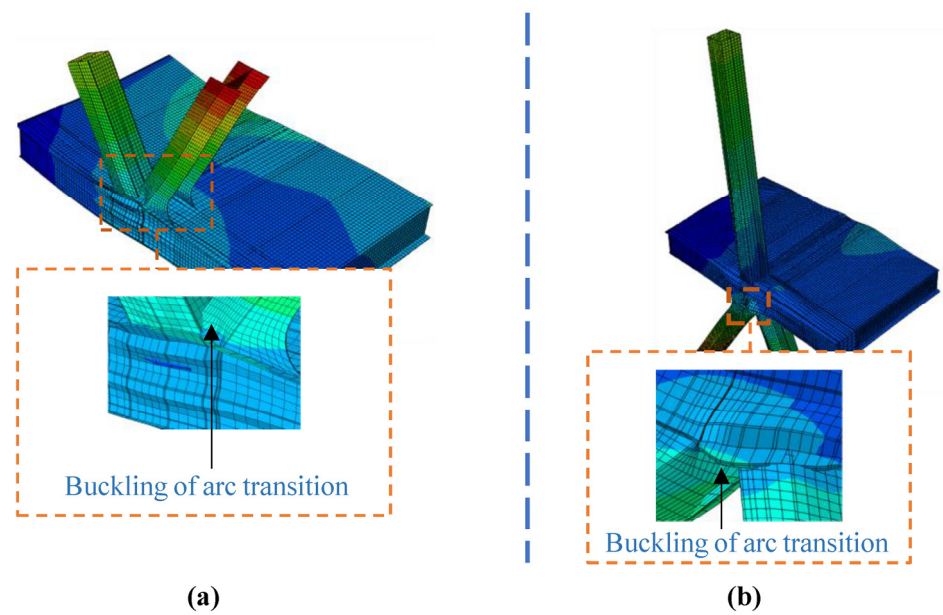


**Figure 32.** Failure modes of novel concrete-filled built-up K-joints with different brace sections: (a) positive bending; (b) negative bending.

**Table 13.** Comparison of the ultimate capacity method and the maximum deformation method for the novel concrete-filled built-up K-joints with different brace sections.

Parameter	Unit Measurement	Positive Bending	Negative Bending
Ultimate capacity	kN	30,285.84	111,830.25
Applied loading	kN	7505.84	42,697.19
Percentage of use of material ( $P_m$ ) based on failure modes	%	28.08	38.18
Percentage of use of material ( $P_m$ ) based on maximum deformation	%	28.97	44.14
Difference between the maximum deformation method and the ultimate load method	%	4.19	5.96

### 3.2. Integral Joint

For both positive and negative bending, the FEM models show the buckling of the gusset plate in the compression brace side (Figure 33). For positive bending, a compression load of 13,250.58 kN causes the structure to fail. The structural analysis shows that the real compression load applied to the structure is 7396.36 kN in the compression brace at the ULS (Table 1). This produces a ratio of 55.81% from the loading comparison. An analysis based on the joint displacement (Table 12) shows that the integral joint has a percentage of use of material of 46.08%. A comparison of these two methods generates a difference of 9.73%, which means that both methods are acceptable.

For negative bending, an axial load of 102,830.72 kN leads to the failure of the dense multi-planar crossbeams. In the ULS, the applied compression load is 58,825.00 kN for negative bending (Table 2). The ratio between these two values shows that the applied loading constitutes 57.20% of the dense multi-planar crossbeams' ultimate strength. Subsequently, based on a displacement limit of  $0.03b_0$ , the loading applied in the structural analysis produces a deformation that represents 46.72% of the deformation limit (Table 12). Therefore, a comparison between these two methods shows a difference of around 10.48% (Table 14), meaning that both methods can be used.

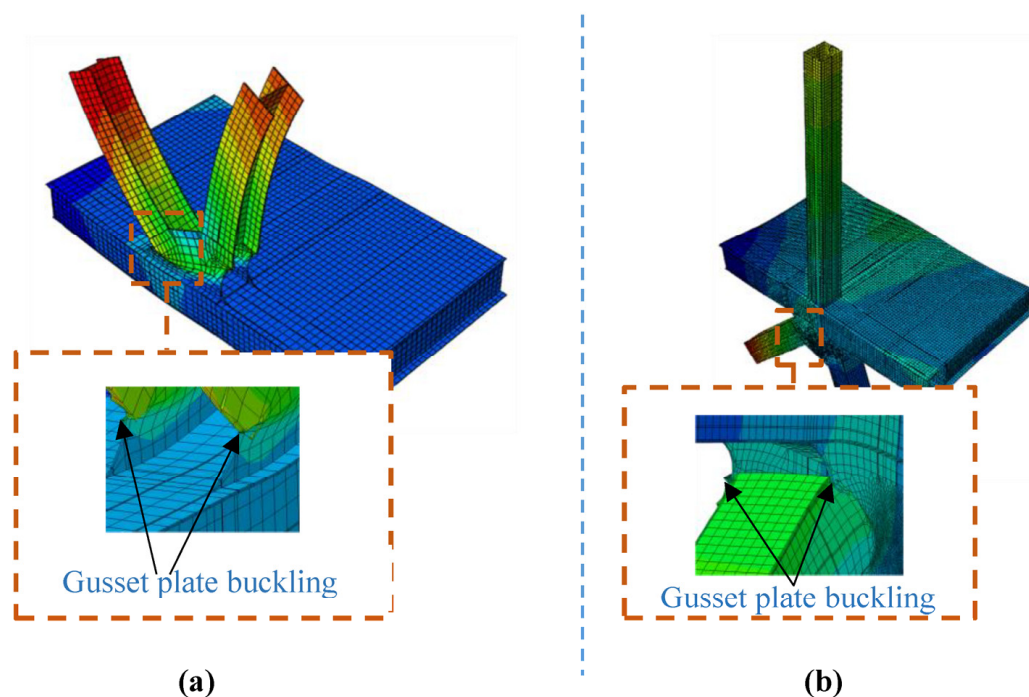


**Figure 33.** Integral joint failure modes: (a) positive bending; (b) negative bending.

**Table 14.** Comparison of the ultimate capacity method and the maximum deformation method for the integral joint.

Parameter	Unit Measurement	Positive Bending	Negative Bending
Ultimate capacity	kN	13,250.58	102,830.72
Applied loading	kN	7396.36	58,825.00
Percentage of use of material ( $P_m$ ) based on failure modes	%	55.81	57.20
Percentage of use of material ( $P_m$ ) based on maximum deformation	%	46.08	46.72
Difference between the maximum deformation method and the ultimate load method	%	9.73	10.48

#### 4. Cost Estimation

In engineering, economy is a fundamental aspect to be considered. For a fair comparison between the novel joint type and the integral joint, cost estimation analysis is carried out in the two types of bending (positive bending and negative bending). In that regard, material price and workmanship are the considered parameters based on the price in China (location of the project) (Tables 15–18).

**Table 15.** Novel joint type in positive bending estimate cost.

Item	Unit	Quantity	Materials		Workmanship		Total	
			Unit Price (CNY)	Amount (CNY)	Unit Price (CNY)	Amount (CNY)	Amount (CNY)	
I			Chord member					
1.1	Steel material	Kg	32,103.36	4.50	144,465.12	2.00	64,206.72	208,671.84
1.2	Stiffeners	Kg	2782.29	4.50	12,520.31	2.00	5564.58	18,084.89
1.3	Concrete infill	m <sup>3</sup>	26.71	3000.00	80,130.00	2000.00	53,420.00	133,550.00
Total chord member								360,306.73
II			Brace members					
2.1	Compression brace	Kg	10,165.60	4.50	45,745.21	2.00	20,331.20	66,076.41
2.2	Tension brace	Kg	6257.89	4.50	28,160.52	2.00	12,515.79	40,676.31
Total brace members								106,752.73
III			Crossbeams					
3.1	Steel material	Kg	17,166.38	4.50	77,248.71	2.00	34,332.76	111,581.47
Total crossbeams								111,581.47
<b>Total cost of novel type of joint in positive bending</b>								<b>578,640.93</b>

**Table 16.** Novel joint type in negative bending estimate cost.

Item	Unit	Quantity	Materials		Workmanship		Total	
			Unit Price (CNY)	Amount (CNY)	Unit Price (CNY)	Amount (CNY)	Amount (CNY)	
I			Chord member					
1.1	Steel material	Kg	32,103.36	4.50	144,465.12	2.00	64,206.72	208,671.84
1.2	Stiffeners	Kg	2782.291	4.50	12,520.31	2.00	5564.58	18,084.89
1.3	Concrete infill	m <sup>3</sup>	26.71	3000.00	80,130.00	2000.00	53,420.00	133,550.00
Total chord member								360,306.73
II			Brace members					
2.1	Compression	Kg	10,165.60	4.50	45,745.21	2.00	20,331.20	66,076.41
2.2	Tension	Kg	6257.89	4.50	28,160.52	2.00	12,515.79	40,676.31
Total brace members								106,752.73
III			Crossbeams					
3.1	Steel material	Kg	17,166.38	4.50	77,248.71	2.00	34,332.76	111,581.47
Total crossbeams								111,581.47
IV			Vertical post					
4.1	Steel post	Kg	2455.48	4.50	11,049.66	2.00	4910.96	15,960.62
Total vertical post								15,960.62
<b>Total cost of novel type of joint in negative bending</b>								<b>594,601.55</b>

**Table 17.** Integral joint type in positive bending estimate cost.

Item	Unit	Quantity	Materials		Workmanship		Total	
			Unit Price (CNY)	Amount (CNY)	Unit Price (CNY)	Amount (CNY)	Amount (CNY)	
I			Chord member					
1.1	Steel material	Kg	32,103.36	4.50	144,465.12	2.00	64,206.72	208,671.84
1.2	Stiffeners	Kg	2782.29	4.50	12,520.31	2.00	5564.58	18,084.89
1.3	Gusset plate	Kg	813.89	4.50	3662.50	2.00	1627.78	5290.27
Total chord member								232,047.00
II			Brace members					
2.1	Compression	Kg	10,165.6	4.50	45,745.21	2.00	20,331.20	66,076.41
2.2	Tension	Kg	10,165.6	4.50	45,745.21	2.00	20,331.20	66,076.41
2.3	Bolts	-	24	0.70	16.80	0.35	8.40	25.20
Total brace members								132,178.02
III			Crossbeams					
3.1	Steel material	Kg	17,166.38	4.50	77,248.71	2.00	34,332.76	111,581.47
Total crossbeams								111,581.47
<b>Total cost of integral joint in positive bending</b>								<b>475,806.50</b>

**Table 18.** Integral joint type in negative bending estimate cost.

Item	Unit	Quantity	Materials		Workmanship		Total	
			Unit Price (CNY)	Amount (CNY)	Unit Price (CNY)	Amount (CNY)	Amount (CNY)	
I			Chord member					
1.1	Steel material	Kg	32,103.36	4.50	144,465.12	2.00	64,206.72	208,671.84
1.2	Stiffeners	Kg	2782.291	4.50	12,520.31	2.00	5564.58	18,084.89
1.3	Gusset plate	Kg	813.888	4.50	3662.50	2.00	1627.78	5290.27
Total chord member								232,047.00
II			Brace members					
2.1	Compression	Kg	8865.35	4.50	39,894.08	2.00	17,730.70	57,624.78
2.2	Tension	Kg	8865.35	4.50	39,894.08	2.00	17,730.70	57,624.78
2.3	Bolt	-	24	0.70	16.80	0.35	8.40	25.20
Total brace members								115,274.76
III			Crossbeams					
3.1	Steel material	Kg	17,166.38	4.50	77,248.71	2.00	34,332.76	111,581.47
Total crossbeams								111,581.47
IV			Vertical post					
4.1	Steel material	Kg	2455.48	4.50	11,049.66	2.00	4910.96	15,960.62
Total vertical post								15,960.62
<b>Total cost of integral joint in negative bending</b>								<b>474,863.85</b>

Tables 15–18 show that the novel joint type is more expensive than the integral joint in both positive and negative bending of the structure. That difference is equal to CNY 102,834.43 for the structure in positive bending and CNY 119,737.70 in the negative bending (Table 19). The main reason resides in the presence of the concrete infill in the chord member for the novel type of joint.

**Table 19.** Estimate cost of the structure in each type of bending and type of joint.

	Unit	Positive Bending		Negative Bending	
		Novel Type	Integral Type	Novel Type	Integral Type
Materials	CNY	388,269.87	329,403.85	399,319.53	328,751.25
Workmanship	CNY	190,371.05	146,402.65	195,282.01	146,112.60
Total	CNY	578,640.93	475,806.50	594,601.55	474,863.85
Difference	CNY	102,834.43		119,737.70	

## 5. Conclusions

For the new project of the Xi'an Weihe bridge, which is located in China, the concept of a dense-crossbeam deck system is adopted and analyzed for the first time in a symmetrical concept. Novel concrete-filled built-up K-joints with different brace sections, which constitute a new type of joint structure, were applied to the aforementioned system and compared to the integral joint (the real joint type in the structure). The results of our analysis generated the following conclusions:

1. Considering the bridge geometry, both the novel concrete-filled built-up K-joints and the integral joint can be applied on the truss structure;
2. The two mentioned joints resist the applied loading under the serviceability limit state and the ultimate limit state. The maximum percentage of use of material is in the latter limit state, equal to 53.47% and 56.19% for the novel joint type and the integral type, respectively;
3. The failure modes of the structure are as expected for both the novel joint type and the integral joint, based on the ultimate capacity analysis. Moreover, a comparison of the aforementioned capacity to the ultimate deformation proposed by the CIDECT code does not show significant differences between the two methods, meaning that they are both accurate in terms of joint analysis;
4. The estimate cost of the novel joint type is higher than the integral joint considering the cost of materials and the workmanship;
5. The behavior of the multi-planar dense crossbeams system should be analyzed in the in-plane bending and the out-of-plane bending, which can be a future study target.

**Author Contributions:** Conceptualization, Y.L.; Methodology, M.N.H.Z.; Software, M.N.H.Z. and X.Z.; Validation, M.N.H.Z.; Formal analysis, M.N.H.Z. and X.Z.; Investigation, L.J.; Data curation, M.N.H.Z.; Writing—oral draft, M.N.H.Z.; Writing—review & editing, Y.L. and L.J.; Supervision, Y.L.; Funding acquisition, L.J. All authors have read and agreed to the published version of the manuscript.

**Funding:** This research was funded by National Science Foundation of China: grant number [52008026], Overseas Students Science and Technology Activities Project Merit Funding in Shaanxi Province: grant number [2021-11]; China Postdoctoral Science Foundation: grant number [2021M692746]; Special Fund for Basic Scientific Research of Central College of Chang'an University: grant number [300102211303].

**Data Availability Statement:** No data were used to support this study.

**Acknowledgments:** The authors would like to address the acknowledgements to the referees for their comments and suggestions, which improved the quality of the present paper. In addition, they express their gratitude to the editor for handling the full submission of the manuscript.

**Conflicts of Interest:** The authors declare no conflict of interest.

## References

1. Ma, Y.; Liu, Y.; Wang, K.; Liu, J.; Zhang, Z. Axial Stiffness of concrete-filled rectangular steel tubular. *J. Constr. Steel Res.* **2021**, *184*, 106820. [\[CrossRef\]](#)
2. Zafimandimby, M.N.H.; Liu, Y.; Yan, B.; Jiang, L.; Ma, Y. Comparison of strengthening methods for tubular T joint corresponding to each static failure mode. *Structures* **2022**, *36*, 589–618. [\[CrossRef\]](#)
3. Ma, Y.; Liu, Y.; Wang, K.; Ma, T.; Yang, J.; Liu, J.; Gao, Y.; Li, H. Flexural behavior of concrete-filled rectangular steel tubular (CFST) trusses. *Structures* **2022**, *36*, 32–49. [\[CrossRef\]](#)
4. Zheng, J.; Wang, J. Concrete-Filled Steel Tube Arch Bridges in China. *Engineering* **2018**, *4*, 143–155. [\[CrossRef\]](#)
5. Packer, J.A.; Wardenier, J.; Zhao, X.L.; Van der Vegte, G.J.; Kurobane, Y. *Design Guide for Rectangular Hollow Section (RHS) Joints under Predominantly Static Loading*; CIDECT: Geneva, Switzerland, 2009.
6. EN 1993-1-8; Eurocode 3: Design of Steel Structures—Part 1-8: Design of Joints. European Union: Brussels, Belgium, 2005.
7. Nassiraei, H.; Lotfollahi-Yaghin, M.A.; Ahmadi, H. Static strength of collar plate reinforced tubular T/Y-joints under brace compressive loading. *J. Constr. Steel Res.* **2016**, *119*, 39–49. [\[CrossRef\]](#)
8. Feng, R.; Chen, Y.; Chen, D. Experimental and numerical investigations on collar plate and doubler plate reinforced SHS T-joints under axial compression. *Thin-Walled Struct.* **2017**, *110*, 75–87. [\[CrossRef\]](#)
9. Chang, H.; Zuo, W.; Xia, J.; Xu, B.; Ma, R.; Zhang, L. Sensitivity analysis of geometrical design parameters on the compressive strength of the vertical inner-plate reinforced square hollow section T-joints: A finite element study. *Eng. Struct.* **2020**, *208*, 110308. [\[CrossRef\]](#)
10. Li, W.; Zhang, S.; Huo, W.; Bai, Y.; Zhu, L. Axial compression capacity of steel CHS X-joints strengthened with external stiffeners. *J. Constr. Steel Res.* **2018**, *141*, 156–166. [\[CrossRef\]](#)
11. Zhu, L.; Zhao, Y.; Li, S.; Huang, Y.; Ban, L. Numerical analysis of the axial strength of CHS T-joints reinforced with external stiffeners. *Thin-Walled Struct.* **2014**, *85*, 481–488. [\[CrossRef\]](#)
12. Gomes, N.V.; de Lima, L.R.O.; da S. Vellasco, P.C.G.; da Silva, A.T.; Rodrigues, M.C. Experimental and numerical investigation of SHS truss T-joints reinforced with sidewall plates. *Thin-Walled Struct.* **2019**, *145*, 105404. [\[CrossRef\]](#)
13. Zafimandimby, M.N.H.; Liu, Y.; Jiang, L.; Ma, Y. Numerical analysis of novel concrete-filled K joints with different brace sections. *Heliyon* **2023**, *9*, e14847. [\[CrossRef\]](#)
14. Cha, H.; Lyrenmann, L.; Connor, R.J.; Amit, H. Varma. Experimental and Numerical Evaluation of the Postfracture Redundancy of a Simple Span Truss Bridge. *J. Bridge Eng.* **2014**, *19*, 04014048. [\[CrossRef\]](#)
15. Gong, X.; Anil, K. Agrawal. Numerical Simulation of Fire Damage to a Long-Span Truss Bridge. *J. Bridge Eng.* **2015**, *20*, 04014109. [\[CrossRef\]](#)
16. Liu, Z.; Li, F.; Roddis, W.K. Analytic Model of Long-Span Self-Shored Arch Bridge. *J. Bridge Eng.* **2002**, *7*, 14–21. [\[CrossRef\]](#)
17. Calçada, R.; Cunha, A.; Delgado, R. Dynamic Analysis of Metallic Arch Railway Bridge. *J. Bridge Eng.* **2002**, *7*, 214–222. [\[CrossRef\]](#)
18. Spyarakos, C.C.; Kemp, E.L.; Venkatareddy, R. Validated Analysis of Wheeling Suspension Bridge. *J. Bridge Eng.* **1999**, *4*, 1–7. [\[CrossRef\]](#)
19. Gunaydin, M.; Sunca, F.; Altunisik C., A.; Ergun, M.; Okur, F.Y. Nonsdestructive Experimental Measurement, Model Updating, and Fatigue Life Assessment of Carsamba Suspension Bridge. *J. Bridge Eng.* **2021**, *27*, 05021017. [\[CrossRef\]](#)
20. Astaneh-Asl, A.; Black, R.G. Seismic and Structural Engineering of a Curved Cable-Stayed Bridge. *J. Bridge Eng.* **2001**, *6*, 439–450. [\[CrossRef\]](#)
21. Gan, X.; Luo, H.; Xu, C.; Yan, L.; Guo, H. Dynamic responses of long-span road-rail cable-stayed bridge under combined seismic and wave action. *Ocean Eng.* **2023**, *270*, 113588. [\[CrossRef\]](#)
22. GB 50157-2013; Code for Design of Metro, Ministry of Housing and Urban-Rural Development. Ministry of Housing and Urban-Rural Development of the People’s Republic of China: Beijing, China, 2013.
23. GB 50090-2006; Code for Design of Railway Line, Railway First Survey and Design Institute. Ministry of Housing and Urban-Rural Development of the People’s Republic of China: Beijing, China, 2006.
24. JTG D60-2015; General Specifications for Design of Highway Bridges and Culverts, Ministry of Transport of People’s Republic of China. Ministry of Transport of the People’s Republic of China: Beijing, China, 2015.
25. JTG D64-2015; Specifications for Design of Highway Steel Bridge, Ministry of Transport of People’s Republic of China. Ministry of Transport of the People’s Republic of China: Beijing, China, 2015.
26. Cheng, B.; Qian, Q.; Sun, H. Steel truss bridges with welded box-section members and bowknot integral joints; Part I: Linear and non-linear analysis. *J. Constr. Steel Res.* **2013**, *80*, 465–474. [\[CrossRef\]](#)
27. Jacob, M.; Balakrishnan S, D. Modal analysis of an RCC long span arch bridge using midas Civil—A validation; materials Today. *Proceedings* **2022**, *57*, 460–463.
28. Wang, T.; Meng, X. The whole modeling and structural seismic analysis of Frame Bridge in Sluice based on Midas Civil. *AIP Conf. Proc.* **2017**, *1829*, 020014.
29. Shi, J.-X.; Ran, Z.-H. Calculation of Creep Effect of Extradosed Cable-stayed bridge based on Midas Civil. *Mater. Sci. Eng.* **2018**, *423*, 012113. [\[CrossRef\]](#)
30. Shi, J.-X.; Ran, Z.-H. Construction simulation analysis of 120 m continuous rigid frame bridge based on Midas Civil. *Earth Environ. Sci.* **2018**, *128*, 012030.
31. Rasmussen, K.J.R.; Young, B. Tests of X and K- Joints in SHS Stainless Steel Tubes. *J. Struct. Eng.* **2001**, *127*, 1173–1182. [\[CrossRef\]](#)

32. Kenedi, W.W. Concrete-Filled—HSS Joints. Master's Thesis, University of Toronto, Toronto, ON, Canada, 1991.
33. Feng, R.; Chen, L.; Chen, Z.; Chen, B.; Roy, K.; Lim, J.B.P. Experiments on stainless steel hybrid K-joints with square braces and circular chord. *J. Constr. Steel Res.* **2021**, *185*, 106865. [[CrossRef](#)]
34. Van der Vegte, G.J.; Makino, Y. Further research on chord length and boundary conditions of CHS T- and X-joints. *Adv. Steel Constr.* **2010**, *3*, 879–890.
35. Huang, W.; Fenu, L.; Chen, B.; Briseghella, B. Experimental study on K-joints of concrete-filled steel tubular truss structures. *J. Constr. Steel Res.* **2015**, *107*, 182–193. [[CrossRef](#)]
36. Hou, C.; Han, L.-H.; Mu, T.-M. Behavior of CFDST to CHS brace composite K-joints: Experiments. *J. Constr. Steel Res.* **2017**, *135*, 97–109. [[CrossRef](#)]
37. Liu, Y.; Zhou, X.; Liu, J. Behavior of concrete-filled rectangular steel tube T-joints and Y- joints under compression. *J. Chang. Univ.* **2007**, *10*, 19721. (In Chinese)
38. Liu, Y.; Zhou, X.; Liu, J. Experiment on Force Performance of Concrete-filled Rectangular Steel tube K-joints. *J. Archit. Civ. Eng.* **2007**, *24*, 36–42.
39. Cheng, B.; Xiang, S.; Zuo, W.; Teng, N. Behaviors of partially concrete-filled welded integral T-joints in steel truss bridges. *Eng. Struct.* **2018**, *166*, 16–30. [[CrossRef](#)]
40. Liu, Y.; Liu, J.; Zhang, J. Experimental research on RHS and CHS truss with concrete-filled chord. *J. Build. Struct.* **2010**, *31*, 86–93. (In Chinese)
41. Gao, Y.; Liu, Y.; Jiang, L.; Liu, J.; Liu, X. Experimental on Flexural Behavior of Rectangular Concrete-filled Steel Tubular Truss Stiffened with PBL. *J. Archit. Civ. Eng.* **2017**, *34*, 171–180. (In Chinese)
42. Chen, Y.; Zhang, S.; Chen, Z. Experimental study on steel reinforced concrete T-section beam subjected to pure torsion and combined action of bending-torsion. *Structures* **2022**, *46*, 1000–1015. [[CrossRef](#)]

**Disclaimer/Publisher's Note:** The statements, opinions and data contained in all publications are solely those of the individual author(s) and contributor(s) and not of MDPI and/or the editor(s). MDPI and/or the editor(s) disclaim responsibility for any injury to people or property resulting from any ideas, methods, instructions or products referred to in the content.